의학박사 학위논문

확률적추적기법의 네트워크 분석을 이용한 조현병 환자의 구조적 뇌 연결성 장애 분석

Structural dysconnectivity in schizophrenia: A subnetwork analysis of probabilistic tractography

울 산 대 학 교 대 학 원

의 학 과

김 하 린

Structural dysconnectivity in schizophrenia:

A subnetwork analysis of probabilistic tractography

지 도 교 수　　이 중 선

이 논문을 의학박사 학위 논문으로 제출함

2022 년　2 월

울 산 대 학 교 대 학 원

의　　학　　과

김 하 린

김하린의 의학박사학위 논문을 인준함

심사위원	김창윤	인
심사위원	김성윤	인
심사위원	주연호	인
심사위원	정범석	인
심사위원	이중선	인

울 산 대 학 교 대 학 원

2022 년 2 월

감사의 글

우선 학위 논문 심사를 해 주신 김창윤 교수님, 김성윤 교수님, 주연호 교수님, 정범석 교수님께 깊은 감사의 말씀을 올립니다. 논문 작성을 위해서 함께 힘써 주신 주성우 선생님, 조영탁 선생님을 비롯하여 모든 연구팀 선생님들께도 감사드립니다. 마지막으로 부족한 저를 변함없는 따뜻함으로 바르게 지도하여 주시고 진심으로 이끌어 주시는 이중선 교수님, 존경하고 항상 감사합니다.

Abstract

Background: The structural network of schizophrenia is characterized by the increased segregation and decreased integration. However, a local deficit in a specific region of interest (ROI) is not sufficient to explain the pathophysiology of schizophrenia. Considering the human brain consists of small-worlds with different connectivity characteristics, the aberrant network structure in schizophrenia should be investigated at a smaller subnetwork level.

Objective: To investigate structural dysconnectivity in two subnetworks of schizophrenia.

Methods: A total of 189 patients and 213 healthy controls were recruited from four different neuroimaging sites. T1 and diffusion-weighted images were used to perform probabilistic tractography, which in turn led to the association matrices of all participants. Network analysis based on graph theoretical approach was then proceeded. Nodal betweenness centrality was used in the k-means clustering algorithm to distinguish two subnetworks from the whole network. Global network properties of schizophrenia and healthy controls were compared in each subnetwork and robustness simulation as well as clinical correlation with network measures were performed.

Results: The subnetwork 1 comprised 75 ROIs with lower betweenness centrality and the subnetwork 2 comprised 12 ROIs with higher betweenness centrality. Patients had an increased level of local efficiency, clustering coefficient, and overall connectivity in the subnetwork 1 whereas these properties as well as global efficiency were decreased in the subnetwork 2. The subnetwork 1 was more robust to sequential nodal damages in patients than controls. The increased network measures in the subnetwork 1 was negatively associated with disease duration.

Conclusions: The central subnetwork (subnetwork 2) was less integrated and segregated

whereas the non-central subnetwork (subnetwork 1) was more segregated, stronger, and vulnerable to targeted damages. The disrupted connectivity in the non-central subnetwork became less prominent while the disease duration increased. We conclude that the integration, segregation, and robustness of structural network in schizophrenia are differently manifested between central and non-central subnetworks.

Key words: schizophrenia, diffusion tensor MRI, tractography, connectivity

List of Tables and Figures

Contents

1. INTRODUCTION

1.1. Schizophrenia as a disconnection syndrome

Schizophrenia is a chronic brain disorder which is characterized by positive symptoms (such as hallucination, delusion) and negative symptoms (apathy, abulia, asociality, alogia) [1]. In early 1900s, Carl Wernicke and Eugene Bleuler suggested the concept of anatomical disruption or splitting of different mental domains in patients with schizophrenia [2, 3]. The sejunction hypothesis in schizophrenia was introduced by Carl Wernicke, which is concordant with the structural dysconnectivity whereas Bleuler's concept of the disintegration of psyche in schizophrenia is concordant with the functional dysconnectivity.

These concepts had been further elaborated and evidenced by recent neuroimaging and electroencephalogram (EEG) studies in which abnormal functional connectivity among brain regions was observed in patients with schizophrenia [4-7]. The term 'disconnection syndrome' was first introduced by Karl Friston and Chris Frith in year of 1995 [8] to explain the possible pathophysiology of schizophrenia, that is, profound disruptions of functional integration between prefrontal and temporal areas were associated with the development of schizophrenia [9]. Because functional integration is determined by proper connections between two or more neuronal systems, a large number of studies were performed to explain functional and structural dysconnectivity in schizophrenia. For example, functional connectivity in frontal regions is consistently reduced in chronic schizophrenia patients when compared to healthy controls [10-12]. Moreover, structural connectivity was reduced in frontal and temporal regions as well as corpus callosum [13-16]. This structural and functional dysconnectivity are also observed in ultra-high risk subjects [17, 18] and patients with first episode psychosis [19, 20], which could be regarded as a potential biomarker of the disorder.

1.2. Probabilistic tractography

The Diffusion-weighted imaging (DWI) is a non-invasive brain imaging method which measures the free motion of water molecules within a voxel. The DWI can measure isotropic and anisotropic diffusion of water molecule in a quantitative manner with apparent diffusion coefficient and fractional anisotropy (FA), which are generated from the restriction of water molecules by cellular structures. Meanwhile, the diffusion tensor imaging (DTI) is derived from the DWI and analyzes diffusion tensor, the three-dimensional shape of the diffusion of water molecule. The DTI of gray matter or white matter tracts is considered as brain structure, therefore, valuable information about the microstructure could be obtained from it [21-33]. For example, the diffusivity measure obtained from the DTI would be changed when certain damages are imposed on neural tissues or disorganization of neural fibers occurs within the tissues. The tractography is an extended three-dimensional model from the DTI which enables researchers to visualize nerve tracts within the brain. Unlike deterministic tractography, probabilistic tractography repeatedly generates thousands of voxel-wise streamlines between brain regions and regards the likelihood of connection as a connection probability [34].

1.3. Graph theory and network analysis

The graph theory is a field of mathematics which simplifies and visualizes pairwise relations between two or more objects. The term ‘graph’ in the theory indicates a combination of multiple points and lines that constitutes a network while focusing on the presence or absence of direct connections between two points [35]. The graph theory enables researchers to analyze big data

more efficiently and to detect connections between specific objects and further explain the importance of connections within the network. The first concept of graph theory was published in 1736 by Leonhard Euler who described the connections of seven bridges between two islands located in the city of Königsberg [35]. The term 'graph' was first introduced by J. J. Sylvester in 1878 [36] and the topic had been further elaborated as a theory since year of 1936 [37]. In recent decades, it has been applied in a variety of fields such as computer science, physics, chemistry, social sciences, economics as well as medicine.

The network analysis is a set of statistical methods based on graph theory, which enables researchers to investigate relations among objects and to analyze network structures derived from these relations. According to the network analysis, any system that can be modelled as a network is considered appropriate to be analyzed. Another advantage of this method is that both quantitative and qualitative information on connections within a given network is available. For instance, studies on genetic co-expression frequently adopt this graph theoretical approach [38] because genetic data obtained from the microarray is suitable for constructing a network. The network can have not only a two-dimensional but also a three-dimensional structure, thus used in the analysis of neuroimaging data.

1.4. Network analysis in schizophrenia

Evidence from preceding research suggests that most brain regions are somehow associated with the pathophysiology of schizophrenia [39]. In other words, a deficit in single brain region is never sufficient to explain the development of schizophrenia. As mentioned above, focusing on the connections within the network derived from structural or functional neuroimaging would be more appropriate to investigate the biological mechanism of schizophrenia.

In this context, efforts have been made to apply graph theoretical approaches to investigate the aberrance of brain network in patients with schizophrenia [30]. For network construction, a structural brain network is typically reconstructed from structural MRIs which include the DTI, diffusion tractography, or even cortical thickness whereas a functional network is reconstructed from the functional MRI (fMRI) or EEG [40]. Both structural and functional networks are closely related because densely clustered cortical structures are well-matched with the specialized brain function of the relevant region [41].

As for the structural network, a specific region of interest (ROI) in the brain is regarded as a node and the connections between two or more nodes are regarded as edges. The global network properties, which are usually considered as criteria for network characteristics, focus on the localization and integration within the overall network. The degree of localization is presented with local efficiency, clustering coefficient, and modularity. On the other hand, the degree of integration is usually presented with global efficiency and/or characteristic path length.

Precedent research on structural dysconnectivity in schizophrenia reported that structural network was disrupted and disorganized in a less effective manner. In short, structural network in schizophrenia is characterized by a higher segregation and a lower integration. First, the clustering coefficient [42] and modularity [43] were increased in schizophrenia, which indicated that the network showed a tendency to cluster and form a separated network units when compared to healthy subjects. Second, the shortest path length was increased in schizophrenia [44, 45], which in turn led to the lower global efficiency in the network [42]. Similarly, schizophrenia patients had a decreased level of global efficiency while local efficiency remained unchanged [46]. In their article, Zhang et al. reported increased

characteristic path length and clustering coefficient in schizophrenia, suggesting a less integrated and more segregated pattern of the network [45]. The decrease of global efficiency in schizophrenia could be explained by the fact that the lesions involving a wide range of white matter have a higher chance of changing the architecture of long white matter tracts. More localized networks would reflect the underlying disruption in the network integrity [47]. As a result, the whole structural network in schizophrenia comprises a significantly higher number of small-world networks because of the disruption of global network properties. In addition, the abnormal hierarchical organization was observed among schizophrenia patients in that the hierarchy of the network was significantly reduced [48].

The brain network "hubs" are important when investigators analyze network properties according to brain regions [49]. The hub is a node which is characterized by high degree and high betweenness centrality within the network. Therefore, the hubs have a greater likelihood of being in the middle of network connections with a lower level of clustering coefficient [50]. The human brain is reported to have hub regions in the fronto-temporal area, corpus callosum, cingulate cortex, insula, and subcortical areas and the lesions of brain disorders were likely to be located in the hubs [51]. In schizophrenia, the centrality was decreased in frontal, temporal, limbic area, and putamen [44, 46].

1.5. Necessity for a subnetwork analysis

Mixed results have been found on the global network connectivity in schizophrenia because of methodological differences. For example, previous studies and a recent meta-analysis showed that patients with schizophrenia had the lower network segregation when compared to healthy subjects [10, 52-55]. However, these results were obtained from either undirected binary graphs

that were reconstructed from the EEG data [53, 54] or fMRI data [10, 55], reflecting a functional connectivity of schizophrenia rather than a structural connectivity.

Because the structural abnormalities in schizophrenia could be subtle at each regional level and the disorder is considered be associated with the aberrant connections between these regions, a network analysis might be more helpful in highlighting subtle structural differences between patients and healthy subjects. This approach enables researchers to compare or summarize network properties more efficiently, because the results reflect a more comprehensive characteristics of the network instead of giving information on network properties obtained from every single ROI. Moreover, the topological network measures could offer researchers insights about network properties which are not available on the single connection level, which suggests the strategy is more suitable when an exploratory investigation or a crude analysis is required [56]. Unlike preceding research which examined the connectivity of the whole structural network, a network analysis at a sub-system level could be more suitable for investigating structural dysconnectivity of schizophrenia. This is because each node could have a different characteristic in terms of connectivity properties or role within the whole structural network. For example, the human brain exists as a combination of small-worlds and is inter-connected through network hubs, regions of high degree and high centrality [57]. In addition, certain connections could be categorized as rich-club connections (i.e. hub nodes to hub nodes) while others as feeder connections (i.e. hub nodes to non-hub nodes) or local connections (i.e. non-hub nodes to non-hub nodes) [58]. As for the graph theoretical approach, network examination at a subnetwork (a distinct cluster of nodes comprising the whole network system) level could be taken into consideration. A subnetwork analysis could be more suitable because exploratory investigation is inevitably necessary because of the complexity of pathophysiology

and the clinical heterogeneity of schizophrenia. A previous study suggested that analyzing brain subnetworks have methodological advantages in that 1) it could reflect the investigator's hypothesis or prior knowledge of schizophrenia and 2) it reduces the number of comparisons and the possibility of the noise variance because not all the values from every ROI are not used [56].

Nonetheless, a significant problem still exists, that is how to identify subnetworks. Several statistical methods were suggested for subnetwork detection, one of which is k-means clustering strategy [59]. Similarly, the degree-corrected stochastic blockmodel which was originated from k-means clustering method has gained its popularity [60, 61] where the edges within the graph are randomly placed between the nodes. Preceding research on subnetworks of schizophrenia reconstructed the functional connectivity from resting-state fMRI [62-64] and performed Ward's method to identify clusters of functional connections based on a Euclidean distance metric or from the gene-based analysis using protein interaction network-based pathway analysis [65, 66]. Drakesmith et al. masked the structural connectivity matrices with spatially and temporally independent subnetworks which were obtained from fMRI data [67]. Another study on structural network examined the network dependency index, a weighted network measure obtained from deterministic tractography, which resulted in four different subnetworks [68]. In addition, the whole structural network derived from the diffusion MRI data were categorized into subnetworks based on the level of centrality, which resulted in central and non-central subnetworks [69]. Betweenness centrality was suggested to be one of significant features that could discriminate schizophrenia patients from healthy controls [70]. Similarly, another preliminary research on graph theoretical approach of functional networks indicated that betweenness centrality was a significant network property which could

discriminate patients from healthy controls [71].

1.6. Purpose of this study

To the best of our knowledge, there is a paucity of literature on the structural networks in schizophrenia which investigated the structural dysconnectivity at each subnetwork level. We aimed to distinguish two subnetworks from the whole structural network based on the level of nodal centrality and to investigate network properties within each subnetwork. In addition, we simulated each subnetwork's stability to sequential nodal damages and observed the association between network properties and clinical characteristics.

2. MATERIALS AND METHODS

The overall processed of our study is shown as a flow diagram in [Figure 1]. After structural MRI data were collected from four different sites, we performed the quality control and preprocessed the obtained neuroimages. The harmonization of diffusion MRI was performed and tested for the performance. Then, an association matrix was obtained from the probabilistic tractography and further used in the graph theoretical analysis. We examined for nodal betweenness centrality and the k-means clustering algorithm was applied to divide two subnetworks from the whole structural network. Global network measures were calculated from each subnetwork and compared between two groups. Lastly, robustness simulation and clinical correlation was investigated.

2.1. Study subjects and further data collection

We collected data of patients with schizophrenia and healthy controls from open public databases as well as one university-affiliated hospital for the large-scale integration of neuroimage data. Each project obtained ethical approval from the Institutional Review Board (IRB) and written informed consent was obtained from all participants.

2.1.1. Asan medical Center

Patients with schizophrenia and healthy subjects were recruited from the department of psychiatry at Asan Medical Center (AMC), a tertiary hospital located in Seoul, Korea. For the patient group, the diagnosis of schizophrenia was established by a board-certified psychiatrist according to the Diagnostic and Statistical Manual of Mental Disorders, Fourth Edition, Text

Revision. Patients who volunteered to participate in the research were required to have presented their first psychotic symptoms within past five years and not to have other psychiatric comorbidities. They were all aged between 20 and 40 years, right-handed, and free of organic brain diseases. We excluded patients when their initial psychiatric diagnosis had changed within 1-6 months during the follow-up periods.

On the other hand, healthy volunteers were enrolled only if they were not diagnosed with any Axis I psychiatric diagnosis. Participants who had any first-degree relative with an Axis I psychiatric diagnosis or those who were unable to complete MRI scanning sessions for any kind of reasons were excluded from this study. Informed consent was obtained from all patients and healthy volunteers. Ethical approval was obtained from the IRB at the AMC.

2.1.2. University of California Los Angeles consortium for neuropsychiatric phenomic LA5c study (UCLA)

The structural MRIs from the UCLA Consortium for Neuropsychiatric Phenomic LA5c study were collected with the accession number of ds000030 at OpenNeuro (openneuro.org). The dataset comprises structural and functional brain MRI of patients with schizophrenia and schizophrenia spectrum disorders, bipolar disorder, and attention-deficit hyperactivity disorder. Moreover, the results of neuropsychological tests and neurocognitive tasks of patient group and healthy controls are included in the dataset [72]. The T1-weighted images (T1-WI) and DWI data of schizophrenia patients and healthy controls were used in this study.

2.1.3. Center for biomedical research excellence (COBRE) and neuromorphometry by computer algorithm Chicago (NMorphCH)

The COBRE and the NMorphCH are freely accessible from SchizConnect (schizconnect.org) [73]. The projects which are included in SchizConnect enables neuroimaging data, neuropsychological test results, and neurocognitive tests to be integrated, which enables researchers to actively participate in the investigations on the neural mechanisms of schizophrenia. As aforementioned, we adopted the T1-WI and DWI data of schizophrenia patients and healthy controls in our study. Those diagnosed with schizoaffective disorder were excluded in further analysis to achieve a higher homogeneity of clinical samples.

2.2. Image acquisition

The MRI data from the AMC were acquired on a 3-Tesla scanner with an 8-channel SENSE head coil (Philips Achieva) while all other neuroimaging data were acquired on a 3-Tesla Siemens Trio scanner.

In the AMC study, the T1□WI was acquired using a turbo field echo sequence and the DWI was obtained via echo-planar imaging sequence for one baseline (b value, 0 s/mm2) and 32 gradient directions (b value, 1,000 s/mm2). In the UCLA study, T1-WIs were acquired with a MPRAGE sequence and DWIs were collected with a slice thickness of 2 mm. In the COBRE study, the coronal T1-WI was acquired with a 12-channel head-coil and a five-echo MPRAGE sequence and the DWI was acquired with a voxel size of 2.0 × 2.0 × 2.0 mm. In the NMorphCH study, the coronal T1-WI was acquired with a 32-channel head coil and a MPRAGE sequence and the DWI was acquired with a 2 mm slice.

The parameters for neuroimage acquisition from all projects are presented in [Table 1].

Table 1. Parameters for neuroimage acquisition

Project	Scanner	Protocol
AMC	3T Philips Achieva	
T1		Field of view (FOV), 240*240*170; voxel size, 1*1*1 mm^3; echo time (TE), 4.6 ms; repetition time (TR), 9 ms; flip angle, 8°
DWI		FOV, 224*224*135 mm; voxel size, 2*2*3 mm^3; TE, 70 ms; TR, 5422 ms; flip angle, 90°
UCLA	3T Siemens Trio	
T1		FOV, 250 × 250 mm; slice thickness, 1 mm; 176 slices; TR, 1900 ms; TE, 2.26 ms; matrix, 256 × 256
DWI		Slice thickness, 2 mm; 64 directions; TR/TE, 9000/93 ms; flip angle, 90°; matrix, 96 × 96; axial slices, b = 0 and 1000 s/mm^2
COBRE	3T Siemens Trio	
T1		TE, 1.64, 3.5, 5.36, 7.22, and 9.08 ms; TR, 2.53 s; TI, 1.2 s; flip angle =

		7°; number of excitations, 1; slice thickness, 1 mm; FOV, 256 mm; resolution = 256 × 256
DWI		TR = 9000 ms; TE = 84 ms; b = 0 and 800 s/mm^2; bandwidth = 1562; 72 slices and 35 directions
NMorphCH	3T Siemens Trio	
T1		TR = 2400 ms, TE = 3.16 ms, flip = 8°, 256 × 256 matrix, 176 slices, slice thickness = 1 mm
DWI		TR = 8000 ms, TE = 86 ms, b = 0 and 800 s/mm^2; flip = 90°, 896 × 896 matrix, 35 slices and 30 directions

AMC: Asan Medical Center, DWI: Diffusion-weighted image, UCLA: University of California Los Angeles Consortium for Neuropsychiatric Phenomic LA5c Study, COBRE: Center of Biomedical Research Excellence, NMorphCH: Neuromorphometry by Computer Algorithm Chicago.

2.3. Quality control of structural and diffusion MRI

First, the T1-WI and DWI obtained from all projects were visually inspected. We detected 28 subjects with signal dropouts and/or artifacts and excluded from further analysis. Second, we used the software SlicerDiffusionQC to remove bad diffusion gradient volume [74]. This software enables researchers to check for the quality of diffusion-weighted MRI. The bad diffusion gradient is determined by comparing distance of each gradient to a median line, which is calculated from the Kullback-Leibler divergence, a measure of difference between two probability distribution. After the automatic processing of the software, we visually inspected the classification result and discarded bad gradient volumes.

2.4. Preprocessing MRI image

After the quality control process, we applied the Psychiatry Neuroimaging Laboratory (PNL) pipeline (https://github.com/pnlbwh/pnlutil) to preprocess DWIs. This pipeline removes oblique coordinate transform (axis alignment) and changes origin to be at the center of the volume (centering). Then, it corrects for motion and eddy current artifacts through affine whole brain registration, with a baseline b = 0 volume using FLIRT in FSL (v 6.0, FMRIB Software, Oxford, UK [75, 76]). We compensated the directions of the gradients for rotations during the affine registration process.

The T1-WIs were parcellated into discrete anatomical regions of interest (ROIs) by the Desikan-Killiany atlas of FreeSurfer V. 6.0. [77, 78]. White and grey matter of each ROI was combined into a single ROI for each anatomical structure. As a result, a total of 87 ROIs across the whole brain were defined in this study. Then, the parcellated T1-WIs were registered to the

DWIs using FLIRT with six degrees of freedom [79]. The list of 87 ROIs is presented in [Table 2].

Table 2. List of regions of interest according to the Desikan-killiany atlas

Regions of interest [a]	Area
Posterior corpus callosum	Corpus callosum
Middle posterior corpus callosum	Corpus callosum
Central corpus callosum	Corpus callosum
Middle anterior corpus callosum	Corpus callosum
Anterior corpus callosum	Corpus callosum
Pallidum	Sub-cortical
Hippocampus	Sub-cortical
Amygdala	Sub-cortical
Thalamus	Sub-cortical
Caudate	Sub-cortical
Accumbens	Sub-cortical
Ventral diencephalon	Sub-cortical
Rostral anterior cingulate	Cingulate
Caudal anterior cingulate	Cingulate
Posterior cingulate	Cingulate
Isthmus cingulate	Cingulate
Banks of superior temporal sulcus	Temporal
Caudal middle frontal	Frontal
Cuneus	Occipital
Entorhinal	Temporal
Fusiform	Temporal
Inferior parietal	Parietal
Inferior temporal	Temporal
Lateral occipital	Occipital
Lateral orbitofrontal	Frontal

Lingual	Occipital
Medial orbitofrontal	Frontal
Middle temporal	Temporal
Parahippocampal	Temporal
Paracentral	Frontal
Pars opercularis	Frontal
Pars orbitalis	Frontal
Pars triangularis	Frontal
Pericalcarine	Occipital
Postcentral	Parietal
Precentral	Frontal
Precuneus	Parietal
Rostral middle frontal	Frontal
Superior frontal	Frontal
Superior parietal	Parietal
Superior temporal	Temporal
Supramarginal	Parietal
Frontal pole	Frontal
Temporal pole	Temporal
Transverse temporal	Temporal
Insula	-

[a] Each region includes left/right hemisphere counter-parts except for corpus callosum

2.5. Diffusion-weighted MRI harmonization

The multi-site diffusion-weighted MRI harmonization is a method which integrates brain MRI data obtained from multiple sites. This method can enable researchers to perform integrated study of various brain diseases and to include more study participants in their research. However, inter-site difference of image acquisition parameters and scanner-specific artifacts limit the possibility of data integration. Therefore, the DWIs should be harmonized by removing scanner-specific differences [80-82].

The retrospective harmonization of raw diffusion images removes scanner-specific differences, which are related to b-values, spatial resolution, and number of gradient directions. On the other hand, it preserves inter-subject anatomical variability. In general, this method is divided into two consecutive steps: a) random sampling of subjects from each study site to learn inter-site differences; b) applying the inter-site differences to all image acquisition sites to harmonize all subjects.

In our study, we assigned the UCLA dataset as a reference site based on the sample size and image parameters while the AMC, COBRE, and NMorphCH dataset were assigned as target sites for harmonization. First, we selected 20 right-handed healthy subjects from the reference site. Second, a subset of 20 right-handed healthy subjects who were matched for age and sex were selected from each target site. All subsets from the reference and target sites comprised solely healthy controls. We compared the subset of the reference site and each target site using unpaired t-test and chi-square test [Table 3].

Table 3. Comparison of subjects from the reference site and each target site for harmonization

Variable	Site		t / χ^2	df	P
	UCLA (n = 20)	AMC (n = 20)			
Age, year, mean (SD)	29.5 (8.2)	29.5 (5.4)	0.000	38	1.000
Sex, male (%)	7 (35)	7 (35)	0.000	1	1.000
	UCLA (n = 20)	COBRE (n = 20)			
Age, year, mean (SD)	29.0 (7.4)	29.0 (7.5)	0.000	38	1.000
Sex, male (%)	8 (40)	8 (40)	0.000	1	1.000
	UCLA (n = 20)	NMorphCH (n = 20)			
Age, year, mean (SD)	31.5 (9.2)	31.5 (9.3)	0.000	38	1.000
Sex, male (%)	10 (50)	10 (50)	0.000	1	1.000

AMC: Asan Medical Center, COBRE: Center of Biomedical Research Excellence, NMorphCH: Neuromorphometry by Computer Algorithm Chicago, SD: Standard Deviation, UCLA: University of California Los Angeles Consortium for Neuropsychiatric Phenomic LA5c Study

Using the dMRIharmonization [80], the b-value mapping was made from original diffusion MRI data and resampling of diffusion images with an unringing method was performed [83]. The scale maps were generated from pairs of rotation-invariant spherical harmonics feature templates, which were derived from spherical harmonic coefficients. The scale maps were then applied to the raw diffusion images of each target site, which in turn resulted in harmonized DWI data. The dMRIharmonization software includes the default options for the procedure (b-value = 1000s/mm^2; resample = 1.53mm^3; spherical harmonic order = 6; number of zero-padding = 10), which were adopted in this study.

We validated the performance of the harmonization by comparing the mean FA value over the whole brain white matter skeleton before and after the procedure. The mean FA value was calculated from the Illinois Institute of Technology Human Brain Atlas v.5.0 (IITmean_FA_skeleton.nii.gz) [84]. The inter-site differences were evaluated using an unpaired t-test.

2.6. Network analysis

2.6.1. Probabilistic tractography

We used the FMRIB's Diffusion Toolbox (FDT) software in the FMRIB's Software Library (FSL) for employing a probabilistic tractography to track white matter streamlines [85]. The diffusion tractography is a non-invasive method that visualizes white matter tracts of the brain [86]. In particular, the probabilistic tractography can generate probabilistic maps for the distribution of fiber orientation at each voxel whereas the deterministic tractography determines streamlines by assigning a fixed direction at each voxel [87]. In other words, the probabilistic tractography generates connectivity distribution at each voxel level. This process is based on the Metropolis-Hastings Markov chain Monte Carlo sampling (bedpostx) [34, 88]. In our study, the probabilistic tracking was performed by a sampling of five thousand streamline fibers at each voxel (probtrackx) [34, 88]. The connectivity probability between the seed ROI and the second ROI was calculated as the number of streamline tracts passing through the second ROI divided by the total number of streamlines. The non-directional connectivity probability between two ROIs was calculated as the average of the probabilities obtained from the tracking of each ROI.

2.6.2. Network reconstruction

The structural networks were reconstructed from the association matrix derived from the probabilistic tractography. The networks were based on 87 ROIs, and the connectivity probabilities between any two ROIs were calculated from the tractography. The reconstructed networks were then transformed as a graph, an ordered pair of edges between nodes. The node

of the association matrix represented each 87 ROIs (nodes of the graph) and the edge represented connections between the nodes, that is, connectivity probabilities. We discarded the connections which were lower than 50% threshold of overall connectivity probabilities in each subject to remove weak or spurious edges. The thresholding value was determined arbitrarily, as it is often applied in previous studies because there is still no consensus or proper null hypothesis [86]. Thresholding could be challenging to This strategy of applying proportional thresholding (density-based thresholding) to all subjects was employed by preceding research [89-91] to remove the same number of weak connections across subjects whereas Hagmann et al. used absolute-thresholding strategy [92]. The connections with the lowest weights are often associated with a higher chance of false-positive network.

2.6.3. Network examination

As aforementioned, we assumed that the whole brain network could be classified into two subnetworks because of the small-world attributes and highly clustered network patterns in structural and functional network of human brain [93]. First, we calculated nodal betweenness centrality of each subject to divide the whole structural network into two discrete subnetworks.

The MATrix LABoratory (MATLAB), a multi-paradigm platform for technical computing, was used to apply brain connectivity toolbox (http://www.brain-connectivity-toolox.net) which enables researchers to calculate a variety number of network properties including nodal network properties (network measure of each ROI) and global network properties [89]. These network measures were based on the non-directional and weighted matrices.

Nodal network properties include (nodal) local efficiency, degree, and betweenness centrality.

Each nodal network properties represents the network connectivity at each ROI level. First, nodal local efficiency is defined as the inverse value of the shortest path length between a given node and direct neighbors. Therefore, the node is considered more efficient when the shortest path length is shorter. Second, nodal degree is defined as the number of all possible connections to a given node. Third, nodal betweenness centrality is defined as the number of shortest paths that passes through a given node in the network. For weighted graphs, the shortest path between two nodes is calculated in the manner that the sum of the weights of the connections is minimized. The betweenness centrality represents the level of a given node's influence in the network. In short, nodal local efficiency reflects the amount of the network segregation [94], while nodal degree and betweenness centrality represent the importance of each node [89, 95].

Global network properties include global efficiency, clustering coefficient, and mean connectivity strength. Each global properties represent the topological characteristics in the whole network. First, global efficiency is defined as the mean of the inverse values of the shortest path length between all possible pairs of nodes. Second, clustering coefficient is the likelihood that connections exist between a given node and its direct neighbors. Third, mean connectivity strength is the average connectivity probabilities of all possible connections. Fourth, the average value of nodal local efficiency and nodal betweenness centrality was calculated. In short, global efficiency reflects network integration [94], clustering coefficient and the averaged local efficiency represents network segregation [96], mean connectivity strength reflects the strength of the entire network [97].

2.6.4. k-means clustering

The k-means clustering is a mathematical algorithm that aims to categorize every observation into k clusters. In this algorithm, clustering is performed repeatedly in an unsupervised manner while each observation is necessarily classified into one of the k clusters with the nearest mean value [98]. A previous study performed the k-means clustering algorithm to identify standardized subsystems from the default mode network [99]. In our study, we defined the nodal betweenness centrality of each 87 ROIs as observations with k = 2. After the k-means clustering, we calculated the global network properties in each subnetwork.

2.7. Robustness simulation

The network robustness is an indicator for the stability under the situation of sequential network damages [100]. To simulate robustness of two subnetworks, we eliminated nodes of all participants one by one in the order of the highest nodal degree. At each nodal deletion process, global network properties were calculated repeatedly. To compare network robustness between patients and healthy controls, a linear mixed-effect model was applied. The number of removed nodes, age, sex, and group (patient or healthy control) was regarded as a fixed effect and each subject was considered as a random effect. The interaction between the number of removed nodes and group, and sex was explored.

2.8. Correlation with clinical characteristics

Patients with schizophrenia were selected for further analysis of associations between clinical variables and network properties. The relationships between network properties and clinical

factors including age, sex, symptom severity, disease duration, and antipsychotic medication were investigated. Only those with known clinical information were analyzed for this statistical analysis. The information about disease duration (year), the dose of antipsychotic medication, and the scores of the Positive and Negative Syndrome Scale (PANSS) was available in the AMC and COBRE dataset [101]. The dose of antipsychotic medication was calculated as the olanzapine equivalent dose (mg/day) [102].

2.9. Statistical analysis

The baseline characteristics between patients and healthy controls were compared by an independent t-test, chi-square test, or Fisher's exact test. The group comparison for network properties was performed by an independent t-test and further adjusted for age and sex in a multivariable linear regression model. Similarly, a linear regression model was reapplied to estimate the relationships between clinical characteristics and each network properties. The independent variables in the regression model included age, sex, disease duration, the PANSS score, and medication dose. For the correction of multiple comparisons, i.e., a total of five regression analysis for each diffusion measure, we used Bonferroni correction. The P value below 0.01 was considered statistically significant in the regression models. The R packages (ver. 4.0.2) were used for statistical analyses [103].

3. RESULTS

Performance of diffusion MRI harmonization

The performance of the harmonization was validated by a comparison of mean FA before and after the procedure. The mean FA value was calculated from the white matter skeleton in the whole brain. The inter-site differences between the reference site and the target site are presented in [Table 4].

Before generating the probabilistic tractography, the mean FA was computed from the resampled diffusion MRI data from the reference sites as well as from the target sites. We excluded a total of 11 subjects whose FA value was 1.5 interquartile range below the first quartile of the mean FA. In total, the study sample comprised 189 patients with schizophrenia and 213 healthy controls.

Table 4. Inter-site differences between the reference and target sites before and after the harmonization

Value	Site		t	P
	UCLA	AMC		
Mean FA (SD)				
Before harmonization	0.495 (0.017)	0.450 (0.016)	8.590	< 0.001***
After harmonization	0.495 (0.017)	0.477 (0.015)	3.454	0.001**
	UCLA	COBRE		
Mean FA (SD)				
Before harmonization	0.489 (0.017)	0.493 (0.015)	−0.938	0.354
After harmonization	0.489 (0.017)	0.490 (0.013)	−0.277	0.783
	UCLA	NMorphCH		
Mean FA (SD)				
Before harmonization	0.494 (0.014)	0.483 (0.047)	1.043	0.304
After harmonization	0.494 (0.014)	0.484 (0.045)	0.941	0.353

AMC = Asan Medical Center; COBRE = Center of Biomedical Research Excellence; FA = Fractional Anisotropy; NMorphCH = Neuromorphometry by Computer Algorithm Chicago; SD = Standard Deviation; UCLA = University of California Los Angeles Consortium for Neuropsychiatric Phenomic LA5c Study

** $P < 0.01$

*** $P < 0.001$

Baseline characteristics

A total of 402 subjects comprising 189 patients with schizophrenia and 213 healthy controls were included in the analysis [Figure 1]. The mean age did not differ significantly between patients and healthy controls (34.1 ± 9.9 vs. 33.7 ± 10.1, respectively; t = -0.374, P = 0.709). More male subjects were included in schizophrenia group without statistical significance (65.6% vs. 59.6 %, respectively; X^2 = 1.529, P = 0.216). Meanwhile, more right-handed subjects were enrolled in healthy control group (90.0% vs. 95.8%, P = 0.024) and the sites for imaging acquisition were significantly different between two groups (P < 0.001) [Table 5].

Figure 1. Flow diagram of network analysis and k-means clustering

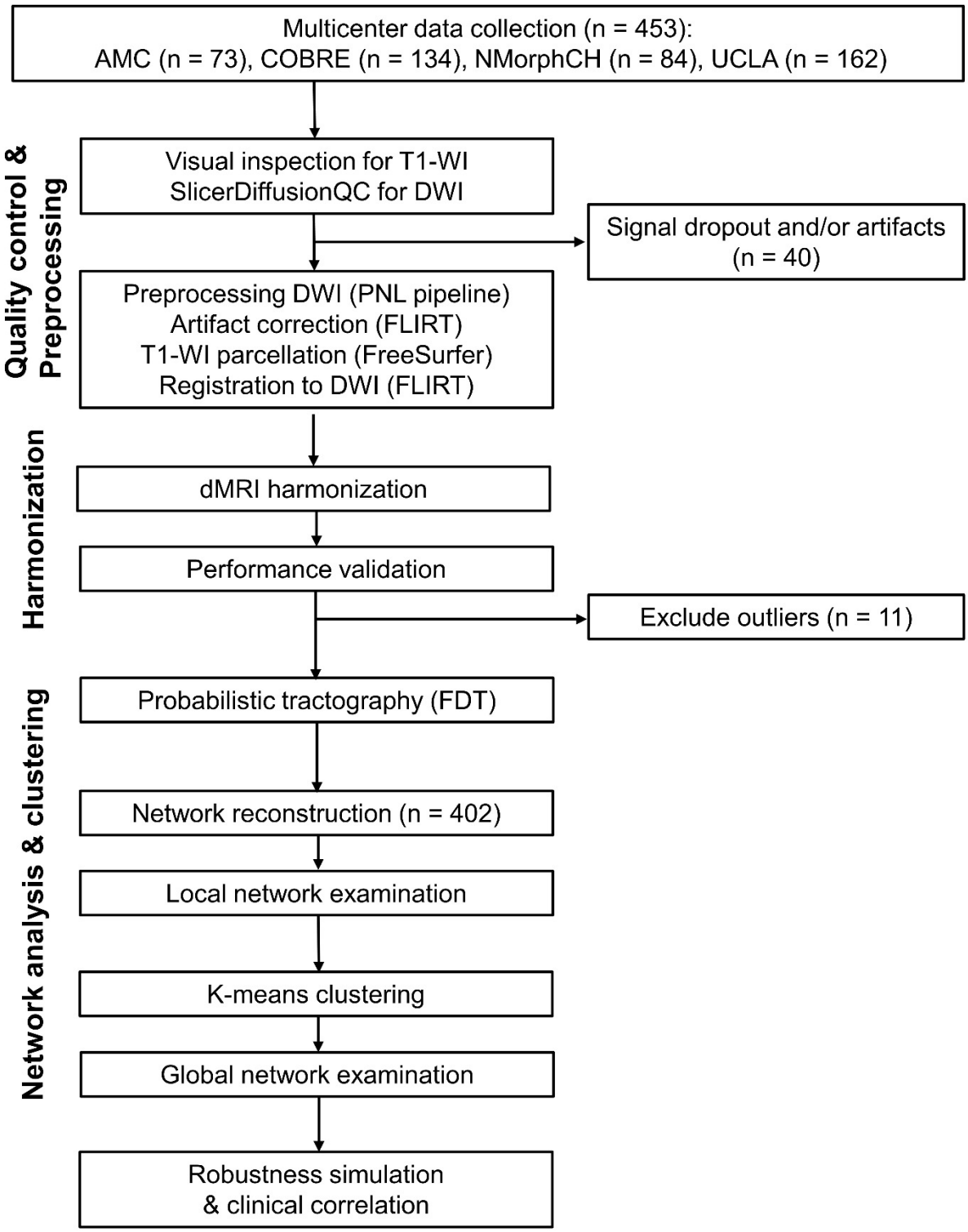

Table 5. Baseline characteristics of patients with schizophrenia and healthy controls

Characteristics	Subjects		Statistical tests	
	SZ (N = 189)	HC (N = 213)	t or X^2	P
Age (mean, SD)	34.1 (9.9)	33.7 (10.1)	-0.374	0.709
Sex			1.529	0.216
Male (N, %)	124 (65.6)	127 (59.6)		
Female (N, %)	65 (34.4)	86 (40.4)		
Handedness [a]				0.024*
Right (N, %)	170 (90.0)	204 (95.8)		
Left (N, %)	13 (6.98)	4 (1.9)		
Both (N, %)	4 (2.1)	5 (2.4)		
NA (N, %)	2 (1.1)	0 (0)		
Imaging sites			23.342	<0.001***
AMC	48 (25.4)	23 (10.8)		
COBRE	57 (30.2)	73 (34.3)		
NMorphCH	40 (21.2)	32 (15.0)		
UCLA	44 (23.3)	85 (39.9)		

[a] Calculated by a Fisher's exact test

SZ = Schizophrenia; HC = Healthy control; SD = Standard deviation; AMC = Asan medical center; COBRE = Center of biomedical research excellence; NMorphCH = Neuromorphometry by computer algorithm Chicago; UCLA = University of California Los Angeles Consortium for Neuropsychiatric Phenomic LA5c Study

* $P < 0.05$

*** $P < 0.001$

Local network analysis and k-means clustering

The nodal betweenness centrality, one of the local network measures was calculated from each ROIs and selected as a variable for further classification of the whole network. As a result, two distinct subnetworks were classified from the whole brain network; the subnetwork 1 consisted of 75 ROIs; the subnetwork 2 comprised 12 ROIs. The nodal betweenness centrality was significantly higher in the subnetwork 2 (mean = 198.0, standard deviation [SD] = 120.6 in the subnetwork 1; mean = 730.0, SD = 240.3 in the subnetwork 2). The mean value of betweenness centrality in each ROI is presented in [Figure 2]. In particular, the subnetwork 2 included anterior and posterior corpus callosum, caudate, pallidum, posterior and isthmus cingulate, and insula in both hemispheres. All other regions were included in the subnetwork 1. The lists of ROIs in the subnetwork 1 and 2 are presented in [Table 6].

Figure 2. Distribution of betweenness centrality in each node from the whole structural network

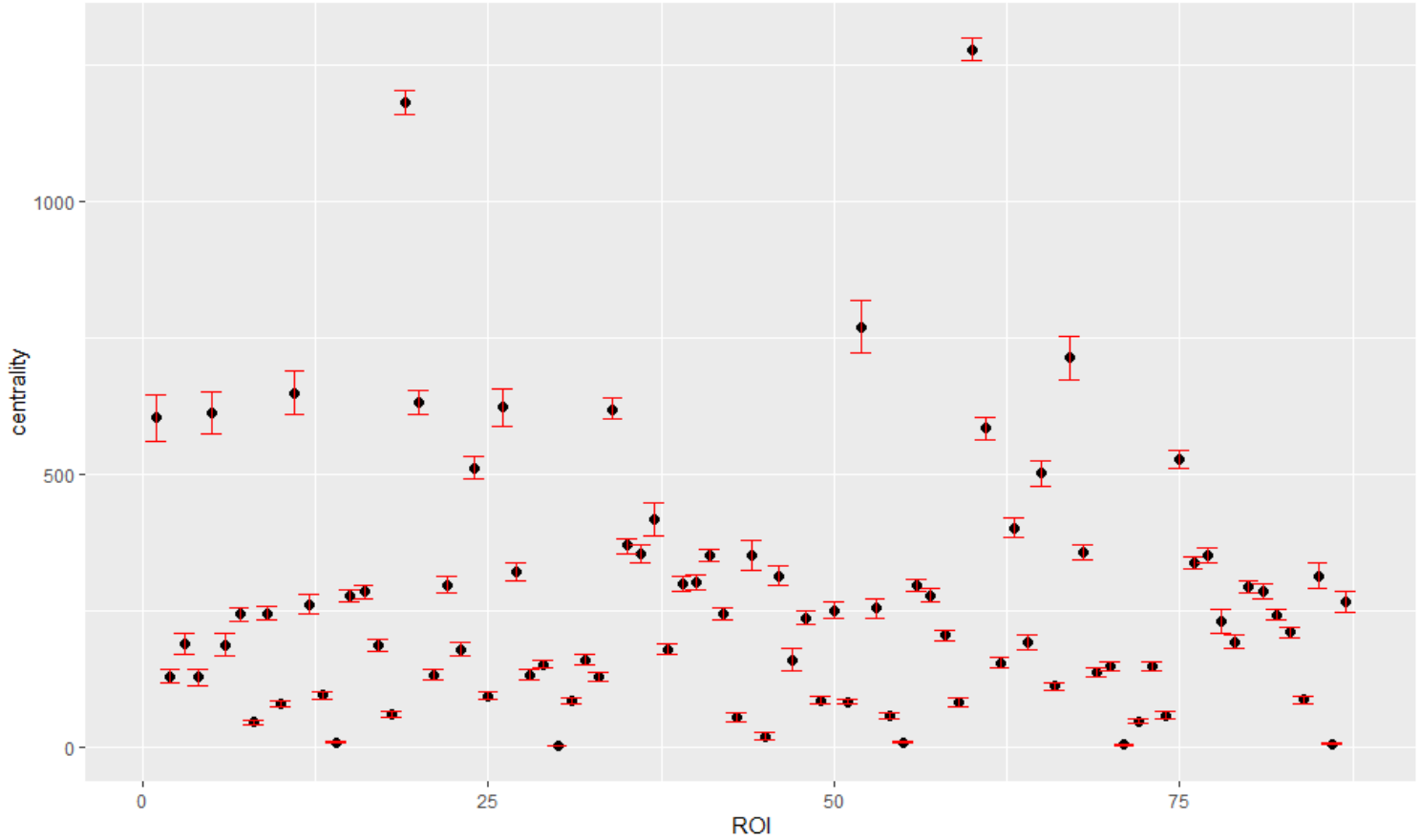

ROI = Region of interest

Mean betweenness centrality is presented with 95% confidence interval

Table 6. Lists of brain regions in each subnetwork after k-means clustering

Subnetwork	Regions of interest [a]	
1	Middle posterior corpus callosum	Medial orbitofrontal
	Central corpus callosum	Middle temporal
	Middle anterior corpus callosum	Parahippocampal
	Hippocampus	Paracentral
	Amygdala	Pars opercularis
	Thalamus	Pars orbitalis
	Accumbens	Pars triangularis
	Ventral diencephalon	Pericalcarine
	Rostral anterior cingulate	Postcentral
	Caudal anterior cingulate	Precentral
	Banks of superior temporal sulcus	Precuneus
	Caudal middle frontal	Rostral middle frontal
	Cuneus	Superior frontal
	Entorhinal	Superior parietal
	Fusiform	Superior temporal
	Inferior parietal	Supramarginal
	Inferior temporal	Frontal pole
	Lateral occipital	Temporal pole
	Lateral orbitofrontal	Transverse temporal
	Lingual	
2	Posterior corpus callosum	Posterior cingulate
	Anterior corpus callosum	Isthmus cingulate
	Pallidum	Insula
	Caudate	

[a] Each region includes left/right hemisphere counter-parts except for corpus callosum

Group comparison of global network properties in each subnetwork

The group comparison of global network measures in each subnetwork is presented in [Table 7]. In the subnetwork 1 (75 ROIs), patients with schizophrenia had a lower level of clustering coefficient (0.016 ± 0.008 vs. 0.018 ± 0.010, P = 0.044) and overall connectivity (0.023 ± 0.005 vs. 0.024 ± 0.006, P = 0.045). Global efficiency (0.073 ± 0.001 vs. 0.074 ± 0.008, P = 0.366), local efficiency (0.020 ± 0.009 vs. 0.022 ± 0.013, P = 0.052), and betweenness centrality (237.756 ± 32.565 vs. 239.153 ± 40.034, P = 0.703) did not show a statistical significance.

In the subnetwork 2 (12 ROIs), reduced global network measures were observed in patients compared with healthy controls. Patients with schizophrenia had a lower level of global efficiency (0.129 ± 0.021 vs. 0.121 ± 0.018, P = 2.11E-05), local efficiency (0.107 ± 0.023 vs. 0.100 ± 0.021, P = 1.54E-03), clustering coefficient (0.089 ± 0.018 vs. 0.084 ± 0.017, P = 4.22E-03), and overall connectivity (0.076 ± 0.012 vs. 0.072 ± 0.010, P = 1.40E-04). Betweenness centrality did not differ significantly between two groups (18.377 ± 4.429 vs. 18.794 ± 4.599, P = 0.356).

Table 7. Comparison of global network properties between patients with schizophrenia and healthy controls in each subnetwork

Network properties	SZ (N = 189)	HC (N = 213)	t	P
Subnetwork 1				
BC (Mean, SD)	239.153 ± 40.034	237.756 ± 32.565	-0.381	0.703
CCo (Mean, SD)	0.018 ± 0.010	0.016 ± 0.008	-2.019	0.044*
GE (Mean, SD)	0.074 ± 0.008	0.073 ± 0.001	-0.905	0.366
LE (Mean, SD)	0.022 ± 0.013	0.020 ± 0.009	-1.952	0.052
OC (Mean, SD)	0.024 ± 0.006	0.023 ± 0.005	-2.015	0.045*
Subnetwork 2				
BC (Mean, SD)	18.794 ± 4.599	18.377 ± 4.429	-0.924	0.356
CCo (Mean, SD)	0.084 ± 0.017	0.089 ± 0.018	2.878	4.22E-03**
GE (Mean, SD)	0.121 ± 0.018	0.129 ± 0.021	4.304	2.11E-05***
LE (Mean, SD)	0.100 ± 0.021	0.107 ± 0.023	3.188	1.54E-03**
OC (Mean, SD)	0.072 ± 0.010	0.076 ± 0.012	3.846	1.40E-04***

*P < 0.05

**P < 0.01

***P < 0.001

SZ = Schizophrenia; BC = Betweenness centrality; CCo = Clustering coefficient; GE = Global efficiency; LE = Local efficiency; OC = Overall connectivity

Multivariable linear regression of global network properties

The multivariable linear regression analysis was performed, which defined age, sex (male as reference), and group (healthy control as reference) as independent variables and each network measure as a dependent variable.

In the subnetwork 1, a significant group difference was found in local efficiency (beta coefficient = 2.76E-03, P = 6.85E-03), clustering coefficient (beta coefficient = 2.51E-03, P = 5.52E-03), and overall connectivity (beta coefficient = 1.40E-03, P = 5.24E-03) in the regression models. The beta coefficients indicated that these network properties had a positive relation with being patient group after adjusting for age and sex. Meanwhile, there was no significant association between group and other network measures such as global efficiency and betweenness centrality (P = 0.094, 0.910, respectively). All regression models were valid with a statistical significance of $P < 0.001$ [Table 8].

In the subnetwork 2, a significant difference between patients and healthy controls was observed in global efficiency (beta coefficient = -7.51E-03, P =3.77E-05), local efficiency (beta coefficient = -5.95E-03, P = 2.77E-03), clustering coefficient (beta coefficient = -4.20E-03, P = 8.11E-03), and overall connectivity (beta coefficient = -3.66E-03, P = 2.27E-04). Unlike the subnetwork 1, a negative association between group and the network measures was observed after adjusting for age and sex. Betweenness centrality, however, did not show a statistically significant difference (P = 0.558). All regression models were valid with a significance of $P < 0.001$ [Table 9].

Table 8. Linear regression model for global network properties in subnetwork 1

Network properties	Coefficient (B)	SE	t	P
BC				< 2.20E-16***
Age	1.134	0.164	6.918	1.83E-11***
Sex (female)	-20.812	3.388	-6.143	1.96E-09***
Group (SZ)	-0.370	3.259	-0.113	0.910
CCo				<2.20E-16***
Age	-2.44E-04	4.52E-05	-5.389	1.22E-07***
Sex (female)	6.22E-03	9.35E-04	6.659	9.16E-11***
Group (SZ)	2.51E-03	8.99E-04	2.790	5.52E-03**
GE				< 2.20E-16***
Age	-1.49E-04	3.33E-05	-4.467	1.03E-05***
Sex (female)	5.95E-03	6.87E-04	8.656	< 2.20E-16***
Group (SZ)	1.11E-03	6.61E-04	1.677	0.094
LE				<2.20E-16***
Age	-2.77E-04	5.11E-05	-5.419	1.04E-07***
Sex (female)	7.05E-03	1.06E-03	6.677	8.21E-11***
Group (SZ)	2.76E-03	1.02E-03	2.718	6.85E-03**
OC				< 2.20E-16***
Age	-1.24E-04	2.50E-05	-4.973	9.83E-07***
Sex (female)	3.66E-03	5.16E-04	7.086	6.30E-12***
Group (SZ)	1.40E-03	4.97E-04	2.808	5.24E-03**

** P < 0.01

*** P < 0.001

SE = Standard error; SZ = Schizophrenia; BC = Betweenness centrality; CCo = Clustering coefficient; GE = Global efficiency; LE = Local efficiency; OC = Overall connectivity

Table 9. Linear regression model for global network properties in subnetwork 2

Network properties	Coefficient (B)	SE	t	P
BC				3.64E-12***
Age	0.123	0.021	5.774	1.82E-05***
Sex (female)	-1.902	0.438	-4.339	1.82E-05***
Group (SZ)	0.247	0.422	0.586	0.558
CCo				< 2.20E-16***
Age	-5.72E-04	7.93E-05	-7.206	2.90E-12***
Sex (female)	9.86E-03	1.64E-03	6.016	4.05E-09***
Group (SZ)	-4.20E-03	1.58E-03	-2.661	8.11E-03**
GE				< 2.20E-16***
Age	-5.63E-04	9.07E-05	-6.206	1.36E-09***
Sex (female)	8.76E-03	1.87E-03	4.672	4.08E-06***
Group (SZ)	-7.51E-03	1.80E-03	-4.168	3.77E-05***
LE				< 2.20E-16***
Age	-7.50E-04	9.95E-05	-7.537	3.27E-13***
Sex (female)	1.22E-02	2.06E-03	5.950	5.86E-09***
Group (SZ)	-5.95E-03	1.98E-03	-3.011	2.77E-03**
OC				< 2.20E-16***
Age	-3.73E-04	4.95E-05	-7.542	3.15E-13***
Sex (female)	6.73E-03	1.02E-03	6.577	1.51E-10***
Group (SZ)	-3.66E-03	9.84E-03	-3.721	2.27E-04***

** $P < 0.01$

*** $P < 0.001$

SE = Standard error; SZ = Schizophrenia; BC = Betweenness centrality; CCo = Clustering coefficient; GE = Global efficiency; LE = Local efficiency; OC = Overall connectivity

Robustness simulation of each subnetwork

The scatter plots showing changes of global network properties during the robustness simulation in the subnetwork 1 and 2 are illustrated in [Figure 2 & 3].

In the subnetwork 1, the robustness simulation showed that betweenness centrality, global efficiency, and overall connectivity had a tendency to decrease continuously as more nodes were sequentially deleted from the subnetwork. Both clustering coefficient and local efficiency increased during the simulation, however, an abrupt decrease in the values was observed after more than 60 nodes were omitted, showing an inverted U-shaped pattern. In schizophrenia, a higher degree of decrement was found in betweenness centrality, global efficiency, and overall connectivity whereas a lower degree of increment was found in other network properties [Figure 3].

In the subnetwork 2, all network properties including betweenness centrality, clustering coefficient, global efficiency, local efficiency, and overall connectivity continuously decreased during the robustness simulation. Unlike the subnetwork 1, a lower level of decrement was observed in patients when compared to healthy controls, except for betweenness centrality that showed a higher decrement in the value [Figure 4].

A linear mixed-effect model was performed to compare the inclination of the change of network properties. The group-by-number of deleted nodes interaction during the simulation was investigated. For the statistical model, the change of network properties was compared until 60th nodes were eliminated from the subnetwork 1 and 10th nodes from the subnetwork 2, considering the linearity shown in the scatter plots.

In the subnetwork 1, a significant group-by-number of deleted nodes interaction was found in global efficiency (coefficient = -5.21E-05, $P < 0.001$, marginal $R^2 = 0.686$, conditional $R^2 = 0.816$). Similarly, a significant interaction was observed in local efficiency (coefficient = -3.73E-05, $P < 0.001$, marginal $R^2 = 0.317$, conditional $R^2 = 0.769$), clustering coefficient (coefficient = -3.05E-05, $P < 0.001$, marginal $R^2 = 0.352$, conditional $R^2 = 0.761$), overall connectivity (coefficient = -4.37E-05, $P < 0.001$, marginal $R^2 = 0.102$, conditional $R^2 = 0.455$), and betweenness centrality (coefficient = -0.150, $P < 0.001$, marginal $R^2 = 0.748$, conditional $R^2 = 0.823$) [Table 10].

In the subnetwork 2, a significant group-by-number of deleted nodes interaction was found in global efficiency (coefficient = 1.15E-03, $P < 0.001$, marginal $R^2 = 0.433$, conditional $R^2 = 0.661$), local efficiency (coefficient = 1.20E-03, $P < 0.001$, marginal $R^2 = 0.335$, conditional $R^2 = 0.581$), clustering coefficient (coefficient = 9.25E-04, $P = 0.004$, marginal $R^2 = 0.255$, conditional $R^2 = 0.528$), overall connectivity (coefficient = 5.12E-04, $P < 0.001$, marginal $R^2 = 0.312$, conditional $R^2 = 0.627$), except for betweenness centrality (coefficient = -0.055, $P = 0.017$, marginal $R^2 = 0.819$, conditional $R^2 = 0.862$) [Table 11].

Figure 3. Global network measures during robustness simulation in subnetwork 1

(a) Betweenness centrality

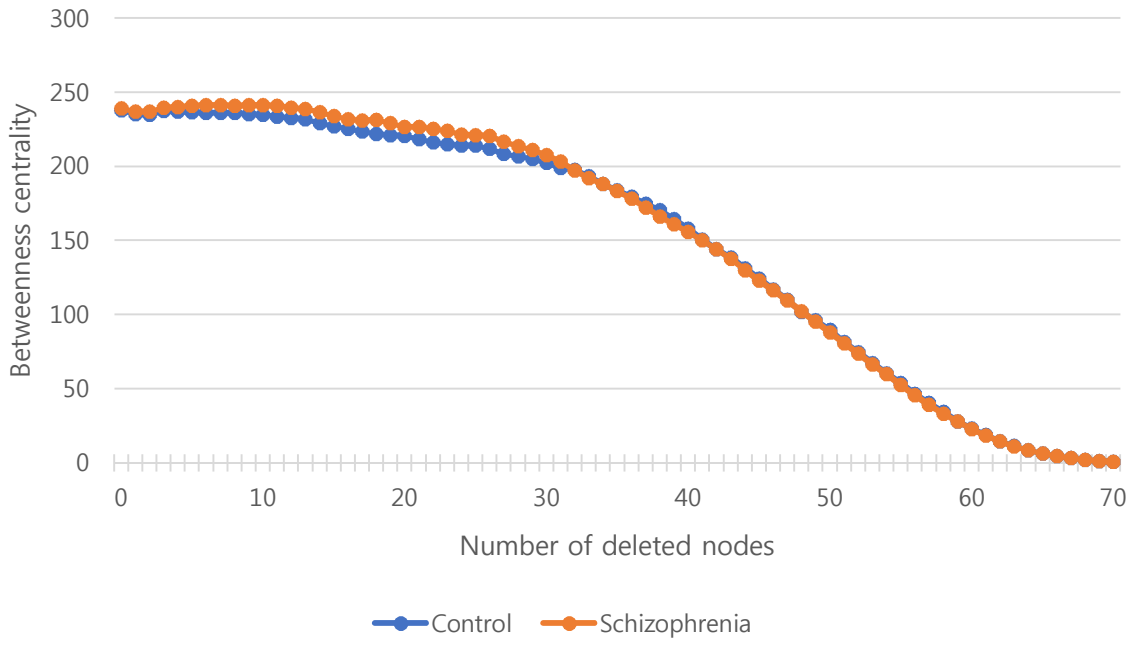

(b) Clustering coefficient

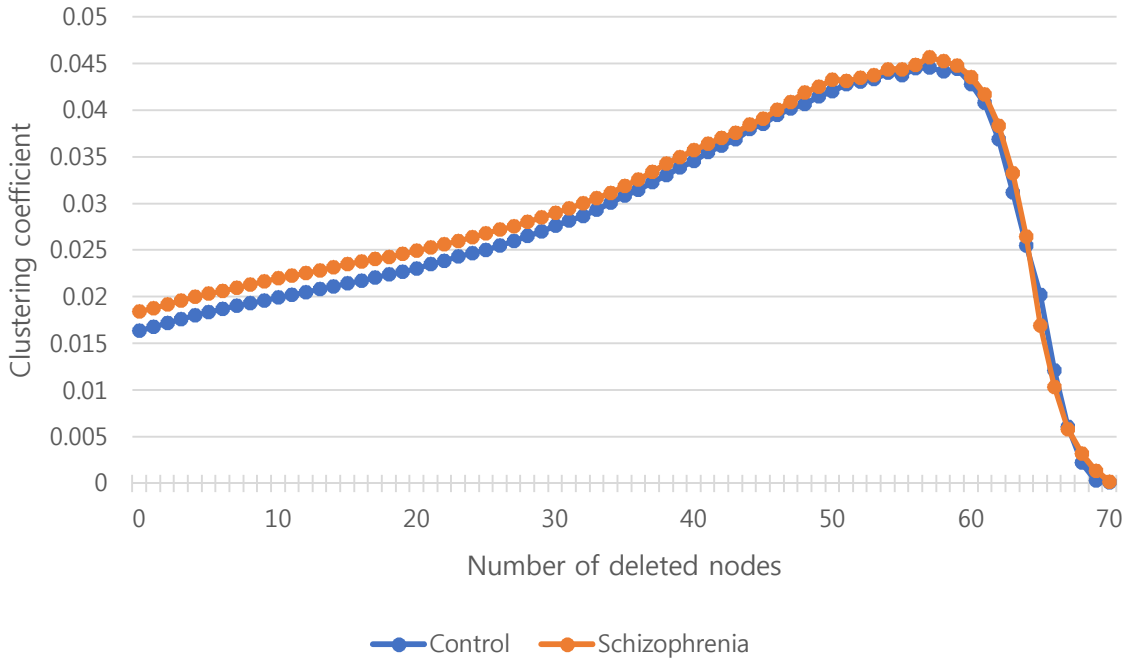

(c) Global efficiency

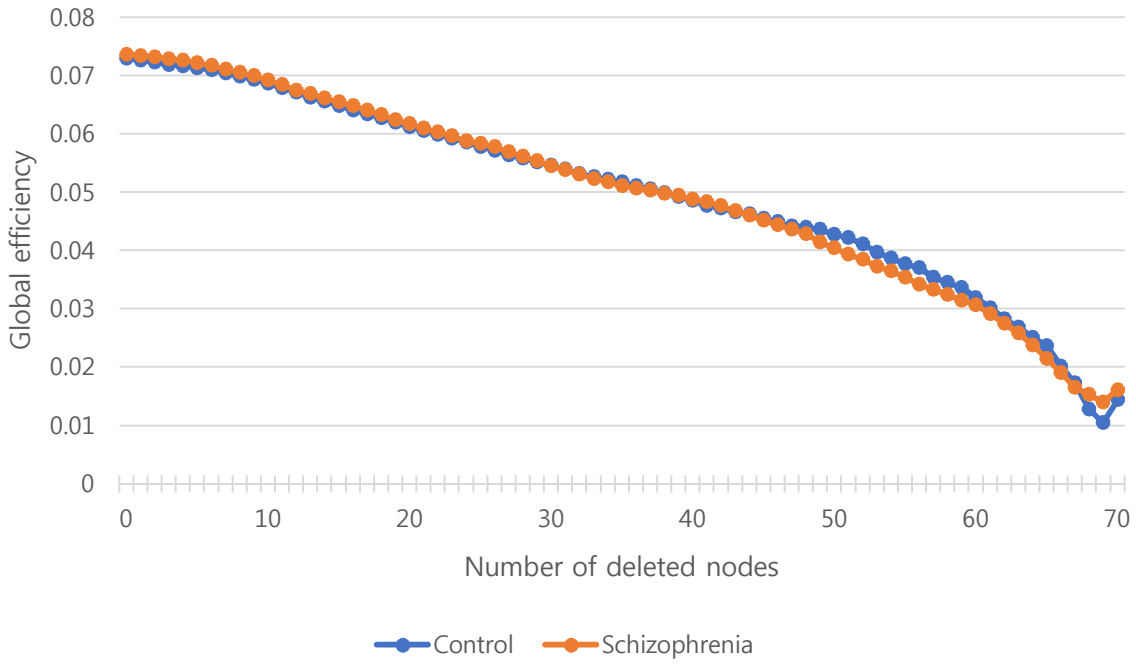

(d) Local efficiency

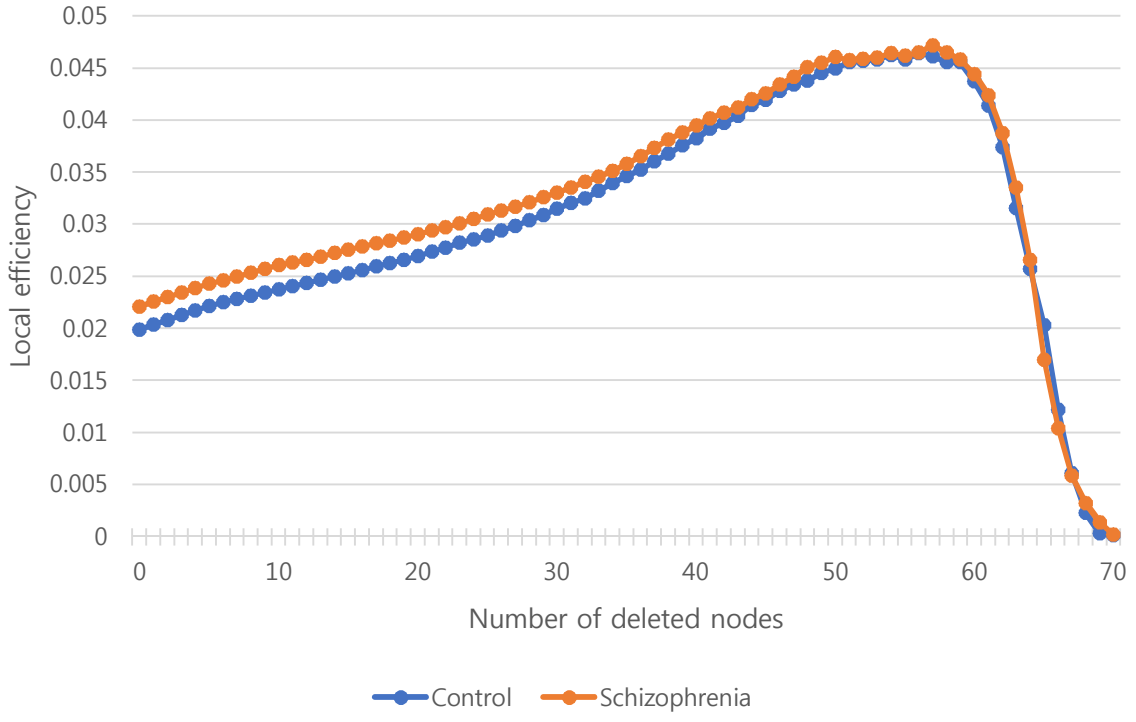

(e) Overall connectivity

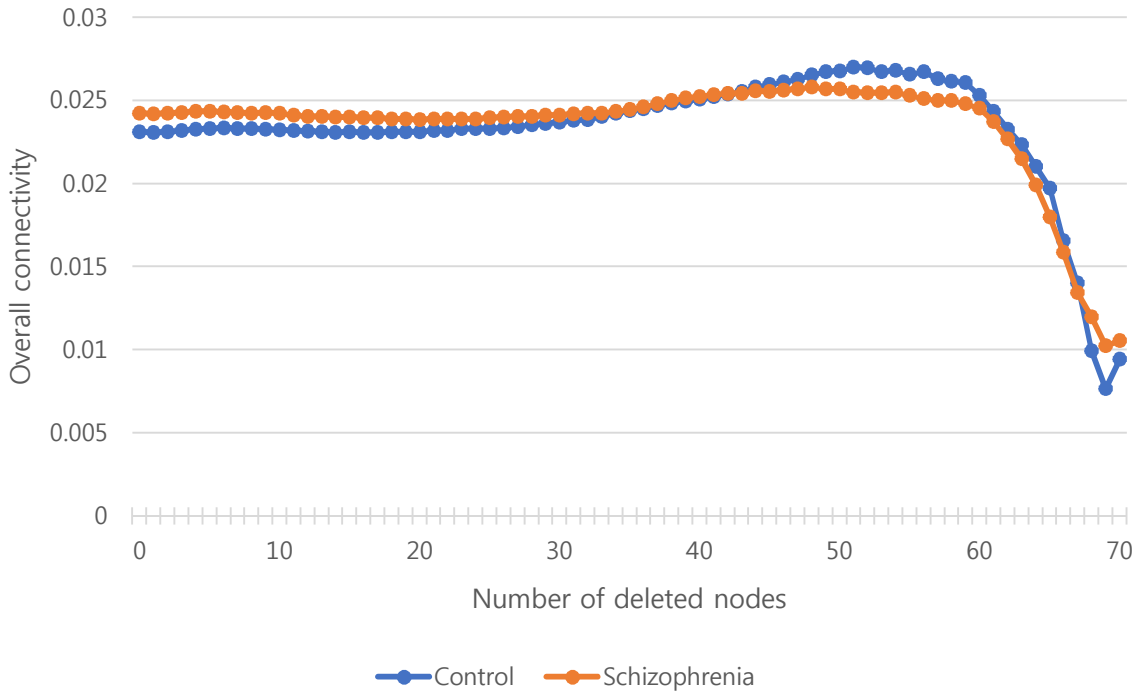

Figure 4. Global network measures during robustness simulation in subnetwork 2

(a) Betweenness centrality

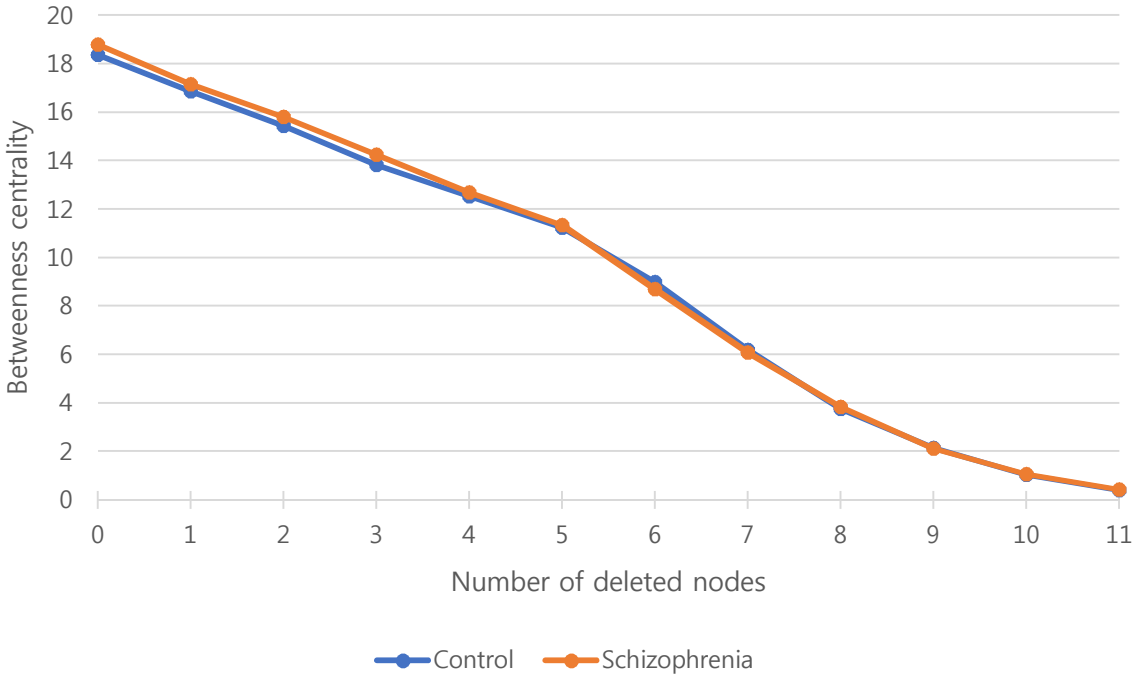

(b) Clustering coefficient

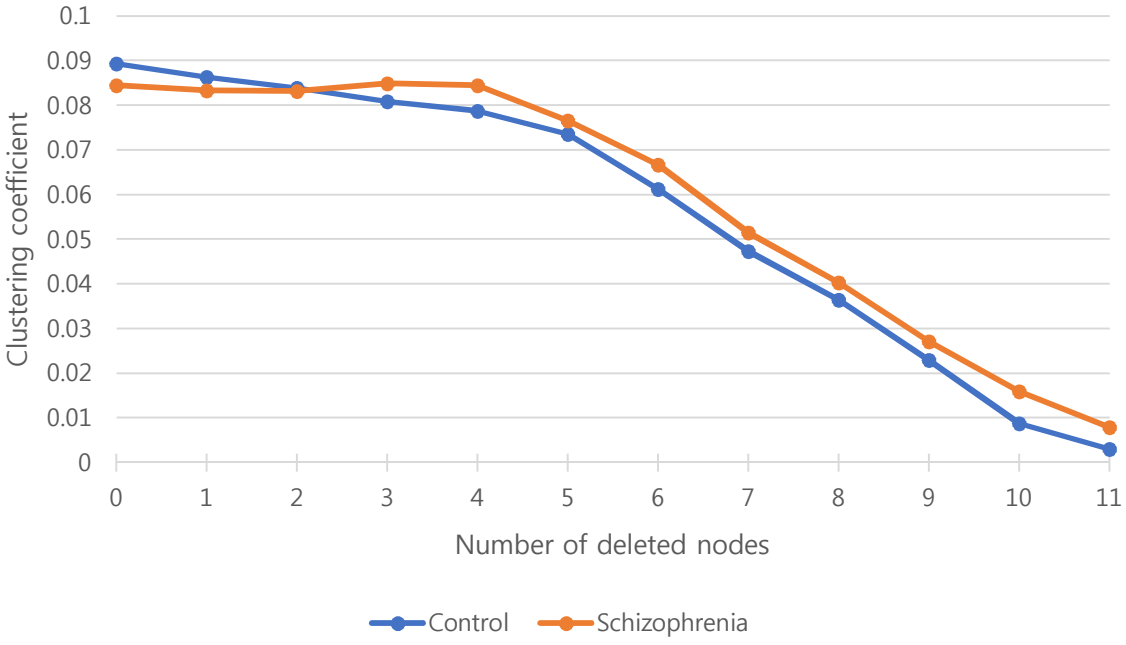

(c) Global efficiency

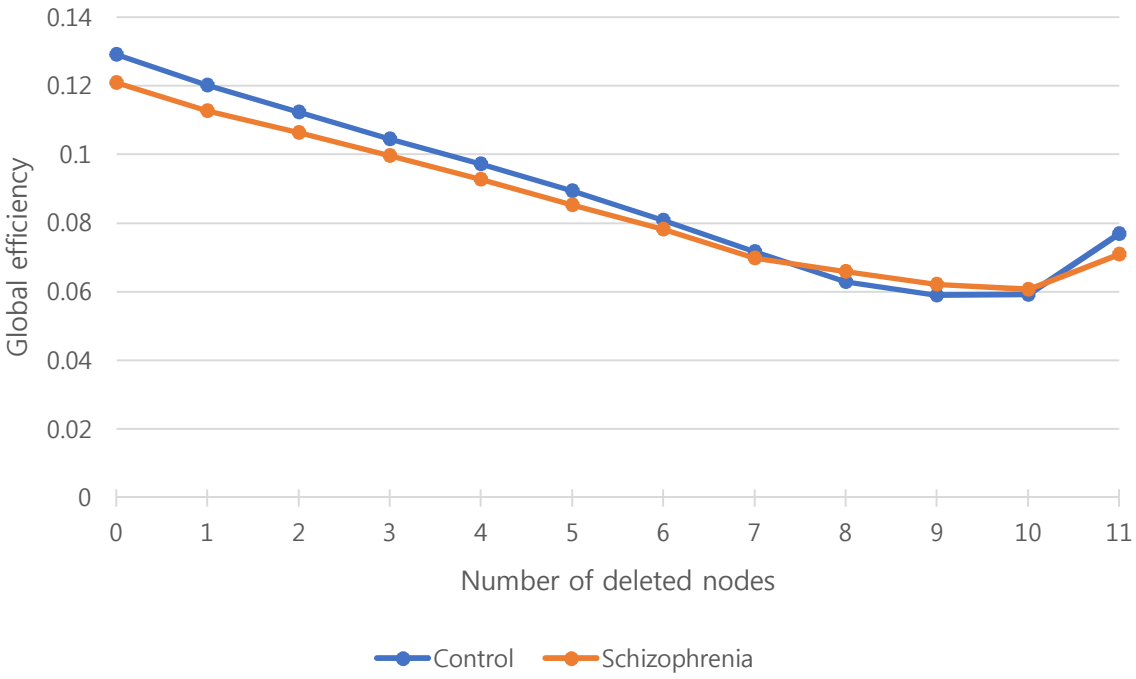

(d) Local efficiency

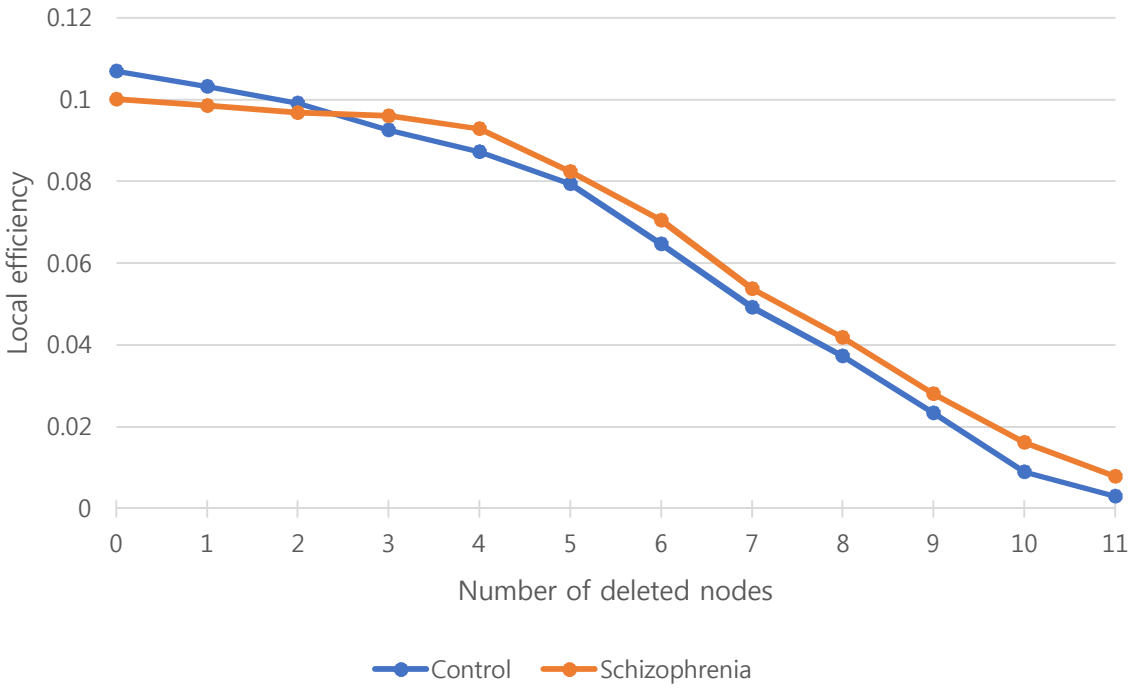

(e) Overall connectivity

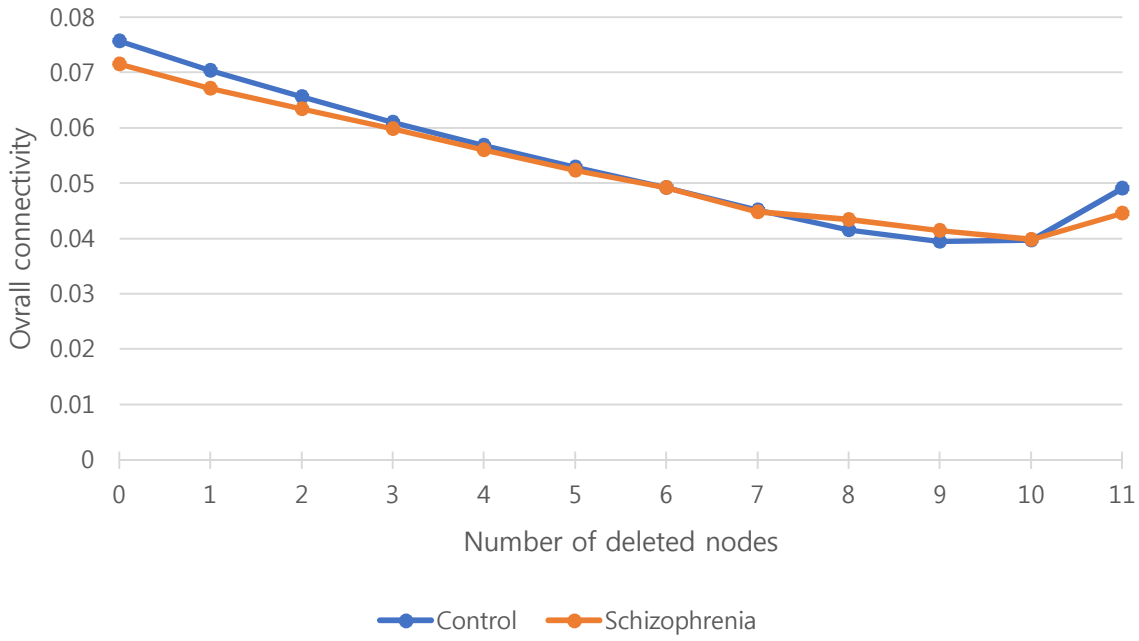

Table 10. Linear mixed effect model for network robustness simulation in subnetwork 1

(a) Betweenness centrality

	Coefficient	SE	t	P
(Intercept)	261.992	5.239	50.006	< 0.001***
Number of deletions	-3.570	1.57E-02	-227.452	< 0.001***
Age	0.645	0.144	4.490	< 0.001***
Sex	-11.186	2.179	-5.134	< 0.001***
Group	5.719	7.460	0.767	0.444
Group * Number of deletions	-0.150	2.29E-02	-6.543	< 0.001***
Group * Age	1.25E-02	0.210	5.95E-02	0.953

(b) Clustering coefficient

	Coefficient	SE	t	P
(Intercept)	1.91E-02	2.76E-03	6.921	< 0.001***
Number of deletions	5.20E-04	4.21E-06	123.598	< 0.001***
Age	-2.41E-04	7.61E-05	-3.168	0.001**
Sex	7.63E-03	1.15E-03	6.618	< 0.001***
Group	6.61E-03	3.94E-03	1.679	0.094
Group * Number of deletions	-3.05E-05	6.13E-06	-4.986	< 0.001***
Group * Age	-1.10E-04	1.11E-04	-0.989	0.323

(c) Global efficiency

	Coefficient	SE	t	P
(Intercept)	7.76E-02	1.35E-03	57.302	< 0.001***
Number of deletions	-6.62E-04	3.18E-06	-208.365	< 0.001***
Age	-1.32E-04	3.72E-05	-3.545	< 0.001***
Sex	3.66E-03	5.64E-04	6.481	< 0.001***
Group	1.23E-03	1.93E-03	0.637	0.525
Group * Number of deletions	-5.21E-05	4.62E-06	-11.255	< 0.001***
Group * Age	1.31E-05	5.43E-05	0.240	0.810

(d) Local efficiency

	Coefficient	SE	t	P
(Intercept)	2.40E-02	2.99E-03	8.026	< 0.001***
Number of deletions	4.90E-04	4.26E-06	115.233	< 0.001***
Age	-2.66E-04	8.23E-05	-3.231	0.001**
Sex	8.34E-03	1.25E-03	6.690	< 0.001***
Group	7.33E-03	4.26E-03	1.722	0.086
Group * Number of deletions	-3.73E-05	6.20E-06	-6.015	< 0.001***
Group * Age	-1.20E-04	1.20E-05	-1.000	0.318

(e) Overall connectivity

	Coefficient	SE	t	P
(Intercept)	2.36E-02	7.24E-04	32.565	< 0.001***
Number of deletions	7.18E-05	1.77E-06	40.582	< 0.001***
Age	-6.18E-05	1.99E-05	-3.110	0.002**
Sex	1.92E-03	3.01E-04	6.369	< 0.001***
Group	1.64E-03	1.03E-03	1.592	0.112
Group * Number of deletions	-4.37E-05	2.58E-06	-16.960	< 0.001***
Group * Age	-4.00E-09	2.90E-05	-1.30E-04	0.095

** $P < 0.01$

*** $P < 0.001$

SE = Standard error

Table 11. Linear mixed effect model for network robustness simulation in subnetwork 2

(a) Betweenness centrality

	Coefficient	SE	t	P
(Intercept)	17.703	0.384	46.078	< 0.001***
Number of deletions	-1.812	1.57E-02	-115.149	< 0.001***
Age	4.86E-02	1.04E-02	4.697	< 0.001***
Sex	-0.608	0.157	-3.876	< 0.001***
Group	0.699	0.547	1.278	0.202
Group * Number of deletions	-5.47E-02	2.29E-02	-2.386	0.017
Group * Age	-1.05E-02	1.51E-02	-0.695	0.488

(b) Clustering coefficient

	Coefficient	SE	t	P
(Intercept)	9.87E-02	6.88E-03	14.357	< 0.001***
Number of deletions	-7.99E-03	2.19E-04	-36.425	< 0.001***
Age	-1.33E-05	1.87E-04	-0.071	0.943
Sex	6.44E-03	2.83E-03	2.273	0.024
Group	1.97E-02	9.79E-03	2.016	0.044
Group * Number of deletions	9.25E-04	3.19E-04	2.898	0.004**
Group * Age	-6.27E-04	2.73E-04	-2.300	0.022

(c) Global efficiency

	Coefficient	SE	t	P
(Intercept)	0.136	4.50E-03	30.223	< 0.001***
Number of deletions	-7.54E-03	1.35E-04	-55.934	< 0.001***
Age	-3.60E-04	1.22E-04	-2.942	0.003**
Sex	8.88E-03	1.86E-03	4.781	< 0.001***
Group	-1.55E-03	6.40E-03	-0.242	0.809
Group * Number of deletions	1.15E-03	1.96E-04	5.857	< 0.001***
Group * Age	-1.90E-04	1.79E-04	-1.061	0.289

(d) Local efficiency

	Coefficient	SE	t	P
(Intercept)	0.118	7.09E-03	16.648	< 0.001***
Number of deletions	-1.00E-02	2.25E-04	-44.538	< 0.001***
Age	-8.17E-05	1.93E-04	-0.423	0.672
Sex	7.97E-03	2.92E-03	2.725	0.007**
Group	1.85E-02	1.01E-02	1.835	0.067
Group * Number of deletions	1.20E-03	3.28E-04	3.652	< 0.001***
Group * Age	-6.40E-04	2.82E-04	-2.272	0.024

(e) Overall connectivity

	Coefficient	SE	t	P
(Intercept)	7.66E-02	3.16E-03	24.251	< 0.001***
Number of deletions	-3.80E-03	8.55E-05	-44.377	< 0.001***
Age	-1.61E-04	8.62E-05	-1.867	0.063
Sex	5.25E-03	1.31E-03	4.016	< 0.001***
Group	3.23E-03	4.50E-03	0.719	0.473
Group * Number of deletions	5.12E-04	1.25E-04	4.110	< 0.001***
Group * Age	-1.83E-04	1.26E-04	-1.456	0.146

** $P < 0.01$

*** $P < 0.001$

SE = Standard error

Correlation with clinical characteristics

A total of 107 patients with schizophrenia were recruited from AMC and COBRE. However, clinical information about either disease duration or the PANSS score was missing or incorrect in 19 subjects. As a result, 88 patients with schizophrenia comprising 57 males (64.7%) and 31 females (35.3%) were included for further analysis. The comparison of clinical characteristics between male and female patients are presented in [Table 12]. Age, the PANSS positive and negative score, and medication dose were not significantly different between male and female patients (36.2 vs. 32.3, P = 0.114; 15.88 vs. 15.74, P = 0.927; 17.46 vs. 15.84, P = 0.240; 15.08 vs. 17.03, P = 0.469; respectively). On the other hand, disease duration was longer in male patients than female patients with a statistical significance (13.67 vs. 6.90, P = 0.009). A Mann-Whitney U test indicated that there was significant difference (W = 1057.5, P = 0.0227) between male and female patients for disease duration.

A multivariable linear regression model was performed to investigate the association between network properties that were significantly different between patients and healthy controls and other clinical factors in each subnetwork. In the subnetwork 1, local efficiency had a significant association with being female (coefficient = 8.51E-03, P = 2.81E-03) and disease duration (coefficient = -6.86E-04, P = 1.21E-04). Similarly, clustering coefficient had an association with being female (coefficient = 7.56E-03, P = 2.80E-03) and disease duration (coefficient = -6.06E-04, P = 1.29E-04). Overall connectivity had a positive association with being female (coefficient = 4.22E-03, P = 2.42E-03) and a negative association with disease duration (coefficient = -3.43E-04, P = 8.60E-05) [Table 13]. All statistical models were valid with a clinical significance at $P < 0.001$.

In the subnetwork 2, global efficiency was significantly associated with age (coefficient = -6.38E-04, P =5.94E-03) whereas local efficiency, clustering coefficient, and overall connectivity were not associated with clinical factors including age, sex, medication dose, disease duration, and the PANSS score [Table 14]. All regression models were statistically significant at $P < 0.01$.

Table 12. Comparison of clinical characteristics between male and female patients with known clinical information

	Male (n = 57)	Female (n = 31)	t	P
Age, yr (SD)	36.2 (12.4)	32.3 (10.2)	1.598	0.114
PANSS-P score (SD)	15.88 (6.56)	15.74 (6.62)	0.092	0.927
PANSS-N score (SD)	17.46 (5.52)	15.84 (6.40)	1.187	0.240
Medication dose, mg/day (SD) [a]	15.08 (11.46)	17.03 (11.83)	-0.730	0.469
Disease duration, yr (SD)	13.67 (13.70)	6.90 (9.78)	2.678	0.009**

[a] Calculated as olanzapine equivalent dose

** $P < 0.01$

SD = Standard Deviation, PANSS-P = Positive and Negative Syndrome Scale-Positive, PANSS-N = Positive and Negative Syndrome Scale-Negative

Table 13. Association between network properties and clinical characteristics in subnetwork 1

	Coefficient (B)	SE	t	P
LE				
Age, yr,	1.07E-04	1.77E-04	0.603	0.548
Sex (female)	8.51E-03	2.76E-03	3.084	2.81E-03**
Medication dose [a], mg/day	-1.27E-05	1.13E-04	-0.112	0.911
Disease duration, yr	-6.86E-04	1.70E-04	-4.044	1.21E-04***
Total PANSS score	-4.99E-05	1.24E-04	-0.401	0.690
CCo				
Age, yr,	9.42E-05	1.58E-04	0.599	0.551
Sex (female)	7.56E-03	2.45E-03	3.086	2.80E-03**
Medication dose, mg/day	-1.20E-05	1.00E-04	-0.119	0.905
Disease duration, yr	-6.06E-04	1.51E-04	-4.027	1.29E-04***
Total PANSS score	-4.40E-05	1.10E-04	-0.398	0.692
OC				
Age, yr,	6.72E-05	8.65E-05	0.777	0.440
Sex (female)	4.22E-03	1.35E-03	3.134	2.42E-03**
Medication dose, mg/day	-8.13E-06	5.52E-05	-0.147	0.883

Disease duration, yr	-3.43E-04	8.27E-05	-4.14	8.60E-05***
Total PANSS score	-2.38E-05	6.07E-05	-0.392	0.696

[a] Calculated as olanzapine equivalent dose

** P < 0.01

*** P < 0.001

SE = Standard error; LE = Local efficiency; CCo = Clustering coefficient; OC = Overall connectivity; PANSS = Positive and negative syndrome scale

Table 14. Association between network properties and clinical characteristics in subnetwork 2

	Coefficient (B)	SE	t	P
GE				
Age, yr	-6.38E-04	2.26E-04	-2.828	5.94E-03**
Sex (female)	4.75E-03	3.51E-03	1.352	0.180
Medication dose [a], mg/day	-2.77E-04	1.44E-04	-1.921	0.058
Disease duration, yr	1.03E-04	2.16E-04	0.477	0.635
Total PANSS score	-4.69E-05	1.58E-04	-0.296	0.768
LE				
Age, yr,	-4.60E-04	2.51E-04	-1.830	0.071
Sex (female)	8.27E-03	3.91E-03	2.116	0.038
Medication dose, mg/day	-3.27E-04	1.60E-04	-2.040	0.045
Disease duration, yr	-4.93E-04	2.40E-04	-2.052	0.043
Total PANSS score	1.44E-04	1.76E-04	0.818	0.416
CCo				
Age, yr	-2.99E-04	2.10E-04	-1.425	0.158
Sex (female)	8.09E-03	3.26E-03	2.480	0.015
Medication dose, mg/day	-2.72E-04	1.34E-04	-2.031	0.046

Disease duration, yr	-4.84E-04	2.00E-04	-2.415	0.018
Total PANSS score	1.50E-04	1.47E-04	1.021	0.310
OC				
Age, yr	-2.16E-04	1.18E-04	-1.833	0.071
Sex (female)	4.62E-03	1.83E-03	2.520	0.014
Medication dose, mg/day	-1.62E-04	7.51E-05	-2.162	0.034
Disease duration, yr	-2.00E-04	1.13E-04	-1.775	0.080
Total PANSS score	9.69E-06	8.26E-05	0.117	0.907

[a] Calculated as olanzapine equivalent dose

** $P < 0.01$

SE = Standard error; LE = Local efficiency; CCo = Clustering coefficient; OC = Overall connectivity; PANSS = Positive and negative syndrome scale

4. DISCUSSION

A total of 402 subjects comprising 189 patients and 213 healthy controls were included in our study. There was no significant difference of age and sex between two groups whereas more right-handed subjects were included in healthy controls. The diffusion MRI harmonization was performed to integrate neuroimaging data from four different projects. The k-means clustering algorithm divided the subnetwork 1 (75 ROIs) and 2 (12 ROIs) from the whole structural network, which was obtained from the probabilistic tractography. The subnetwork 2 included anterior and posterior corpus callosum, caudate, pallidum, posterior half of cingulate, and insula in both hemispheres. In the subnetwork 1, patients had a higher level of clustering coefficient and overall connectivity when compared to healthy controls while they had a lower level of clustering coefficient, local efficiency, global efficiency, and overall connectivity in the subnetwork 2. After adjusting for age and sex, clustering coefficient, local efficiency, and overall connectivity were higher in schizophrenia in the subnetwork 1 whereas clustering coefficient, local efficiency, global efficiency, and overall connectivity were lower in the subnetwork 2.

The robustness simulation and a linear mixed-effect model indicated that a more abrupt decrease was observed in betweenness centrality, global efficiency, and overall connectivity while a more gradual increase was found in local efficiency and clustering coefficient in the subnetwork 1 of schizophrenia group. On the other hand, global efficiency, local efficiency, clustering coefficient, and overall connectivity decreased more slowly in the subnetwork 2.

Among all participants, 88 patients with known clinical information were included in the further analysis. Approximately two-thirds of the patients were male although there was no significant difference of age, the PANSS score, and daily medication dose between male and

female patients, except for disease duration. In the subnetwork 1, a significant negative association was observed between disease duration and network properties such as local efficiency, clustering coefficient, and overall connectivity while a positive association was observed between these network properties and being female. In the subnetwork 2, only age was negatively associated with global efficiency when adjusting for all other variables.

Betweenness centrality, one of centrality measures in network analysis was used to discriminate two subnetworks in our study. This approach had rationales as follows: First of all, previous studies on graph theoretical analysis suggested betweenness centrality serves as an important feature that could distinguish schizophrenia patients from unaffected subjects [70, 71]. Second, patients with schizophrenia have a decreased level of betweenness centrality in the whole structural network [104] as well as in a specific ROI such as parietal hub [105] and frontal hub [44], which are suggested to be associated with the symptom manifestation of schizophrenia [106]. Lastly, the centrality measure at a specific ROI was decreased in certain nodes while it was reversely increased in other regions, indicating the less optimal organization of structural network in schizophrenia [45]. Therefore, we categorized every node into either the subnetwork 1 or the subnetwork 2 according to the betweenness centrality at each ROI's level.

Our results showed that a distinct subnetwork could be distinguished from the whole structural network. A smaller subnetwork, namely the subnetwork 2, consisted of 12 ROIs; anterior and posterior corpus callosum, caudate, pallidum, posterior half of cingulate, and insula in both hemispheres. These brain regions were considered to have a higher nodal betweenness centrality when compared to other regions from the subnetwork 1. Therefore, the group of nodes (12 ROIs) characterized by high centrality could be regarded as "hubs" in the structural network. The hubs are group of nodes that have a high level of nodal degree and betweenness

centrality and are considered be in the middle of network connections and thus responsible for the control of information flow within the network [49]. There is evidence that central hubs exist in fronto-temporal, limbic, paralimbic, and subcortical areas of human brain [107-110]. The nodes with high centrality in the subnetwork 2 were in line with a previous study that showed brain regions with high betweenness centrality included major white matter tracts that included corpus callosum, cingulum, and several projections connecting the subcortical areas with cortical areas such as caudate nucleus, insula, and pallidum [111]. However, other central regions such as frontal and parietal hubs were not included in the subnetwork 2. This may be the result of methodological differences and heterogeneity of study participants. For example, several human brain hubs such as superior frontal, superior parietal, and precuneus [112] were not categorized as the subnetwork 2 despite the high value of betweenness centrality because the number of clusters from k-means clustering algorithm was arbitrary.

We examined the structural connectivity in each subnetwork because both central and non-central subnetworks could be associated with schizophrenia. Alloza et al. suggested that a characteristic of schizophrenia is an alteration of structural connectivity that is found not only in brain hubs but also in non-central regions [69]. In other words, the structural connectivity abnormalities of the average network derived from the whole brain are caused by central and non-central subnetworks. While most preceding research focused on structural dysconnectivity in hub nodes [45, 48], they emphasized the role of non-central networks because the role of hubs might be replaced by other brain regions because of the apparent hierarchical disorganization of schizophrenia [48]. In other words, schizophrenia should be considered in the context of the imbalanced connectivity within each subnetwork. In this point of view, the different network connectivity observed in the subnetwork 1 and 2 could reflect the imbalanced

connections within each small-worlds.

In the subnetwork 1, patients had a higher level of local efficiency and clustering coefficient. Because these network properties reflect the degree of network segregation, patients with schizophrenia were thought to have a more localized subnetwork 1 when compared to healthy controls. Moreover, overall connectivity, a measure for the strength of overall connections, was higher in schizophrenia patients, which suggested that the connections within the subnetwork 1 were stronger. Considering the subnetwork 1 consisted of a majority of the nodes in the whole network, this finding was in line with previous studies that the structural network in schizophrenia is more segregated than in healthy subjects [42, 45]. Unlike preceding research which suggested a less integrated connectivity pattern in schizophrenia, global efficiency did not show a significant difference between two groups in our study. This discrepancy could happen because the subnetwork 1 did not include many nodes with high centrality. In other words, deficits of white matter tracts with many connections (i.e. the subnetwork 2) could disrupt the network integration in both patients and healthy controls [47, 107].

In the subnetwork 2, local efficiency, clustering coefficient, global efficiency, and overall connectivity was lower in schizophrenia. In other words, patients had a less segregated and integrated, and weaker network connections within the subnetwork 2. When highly central nodes are closely connected among themselves, the group of nodes can be termed “rich-club”, meaning the highly interconnected club of nodes with rich connections [113]. The human brain’s rich club was detected in frontoparietal hubs as well as other regions including cingulate cortex and insula [43, 113]. Therefore, the subnetwork 2 in our study could also be regarded as a rich-club organization although frontoparietal cortical hubs were not included. This disparity might happen owing to methodological differences or even be derived from the decrease of the

number of hubs which is observed among schizophrenia patients [44-46, 114]. The disruption of this rich club organization was suggested to interfere with the whole brain's integrity because it is responsible for the appropriate information flow among remote brain regions [115]. Our results were consistent with previous reports that global efficiency was lower [44, 116] and connectivity was decreased [117] in the rich club of schizophrenia. The less segregated network characteristics in the subnetwork 2 was also thought to reflect the aberrant structural dysconnectivity in schizophrenia. To the best of our knowledge, however, little is known about the impact of impaired segregation on the rich club. Moreover, caution must be taken when interpreting our results because the subnetwork 2 comprised a small number of nodes, which could limit the possibility of further analysis of network properties at a smaller regional level.

Each ROIs included in the subnetwork 2 could be further understood at the regional level. First, structural abnormalities of corpus callosum in schizophrenia had been consistently reported since year of 1994 [118, 119]. Diffusion tensor imaging revealed that patients had a reduced level of FA in the splenium of corpus callosum [120, 121]. However, there was a lack of literature on structural connectivity of corpus callosum in schizophrenia although patients with bipolar affective disorder had a decreased level of global and local efficiency in their structural networks, of which the impaired network organization was most prominent in corpus callosum [122]. Second, a decreased level of network segregation and integration was observed in basal ganglia of schizophrenia patients [123, 124]. This region was also associated with the decreased functional connectivity according to a recent meta-analysis [125]. Third, the aberrance of structural connectivity was observed in posterior cingulate of schizophrenia patients where the mixed results for functional connectivity were reported in the same region [99, 126]. This discrepancy might be regarded as a core pathophysiology of schizophrenia, that is the

decoupling of structural and functional connectivity in posterior cingulate. On the other hand, functional connectivity in schizophrenia would be more complex than structural connectivity although they are closely related to each other [127, 128]. Fourth, insular hub was suggested to be the most severely damaged ROI in a previous study on structural network of schizophrenia. Specifically, the connection strength was decreased in the region, which was in accordance with our results [110]. Insula has a wide range of bidirectional connections to other brain cortices and limbic areas and integrates external sensory stimuli such as auditory or visual stimuli, information with emotional value, and somatic pain. Therefore, psychotic symptoms could occur when insula is damaged because the affected person loses the ability to integrate enormous amount of information or to relate to other person's emotional experiences [129, 130].

As more nodes were sequentially excluded from the subnetwork 1, a gradual decrease was detected in betweenness centrality, global efficiency, and overall connectivity, indicating that the integrity and strength of the subnetwork and overall importance of 75 nodes were disrupted from the additive damages. The decrement was more prominent in patients with a statistical significance, which reflected the vulnerability of the subnetwork 1 in schizophrenia [100]. Our results were consistent with previous studies which showed the structural connectivity was more vulnerable to either random or targeted damages in schizophrenia patients [123, 131]. Meanwhile, local efficiency and clustering coefficient, the network properties implying the degree of network segregation continuously increased, indicating that the subnetwork 1 became not only less integrated but also more segregated during the simulation. The increment was more profound in healthy subjects than in patients. This gap between two groups was thought to occur because the subnetwork 1 of patients was already more segregated before any nodal

damage. After more than 60 nodes were eliminated, an abrupt change of network properties was detected, which was probably an error derived from the small number of residual nodes.

Robustness simulation of the subnetwork 2 showed that all network measures declined as more nodes were eliminated, meaning that targeted damages induced the disruption of the structural connectivity. The subnetwork 2 was considered more robust in schizophrenia patients than in healthy controls because the decrease of network properties was more prominent in healthy participants. There is evidence that schizophrenia patients have a more robust structural network; their network measures remained stable during the simulation of targeted damages [132] or random damages [10]. This phenomenon was also observed among childhood-onset schizophrenia or unaffected relatives of schizophrenia patients [132, 133]. The stableness of network properties in schizophrenia was suggested to be associated with a compensation for the disrupted local networks [133] and might have a survival benefit from the local brain damages [10]. However, most preceding research on the network robustness was based on fMRI data [10, 132, 133], and adopted a binary, undirected graph or evaluated the robustness only with the global efficiency [132]. As aforementioned, the interpretation of the result should be made with caution because the subnetwork 2 consisted of a smaller number of nodes.

The clinical correlation with network properties showed that disease duration had a negative association with local efficiency, clustering coefficient, and overall connectivity in the subnetwork 1. The longer the duration of illness, the weaker and less segregated network connectivity in the subnetwork 1. This was in accordance with a previous study in that the decrease of local efficiency, clustering coefficient, and connectivity strength was associated with the duration of schizophrenia [55]. Palaniyappan et al. suggested that the change of the structural connectivity in non-hub regions can occur because of cortical reorganization which

is a compensatory mechanism for the diminished central role of brain hubs [10, 123] where the progressive structural changes are profound during the early phase of schizophrenia [134]. In other words, the difference of network properties in non-central regions, that is the subnetwork 1, is evident in early schizophrenia and decreases with the longer disease duration. It is further evidenced by previous suggestions that the progressive change of brain structure occurs during the first two years after the development of schizophrenia [135, 136]. When we assumed the increased segregation and strength in the subnetwork 1 of schizophrenia as a reactive change as discussed before, this compensation was considered to decrease with the longer duration of illness. Indeed, disease duration of the patients in the AMC was mostly less than two years. Moreover, female patients had a higher level of network measures in the regression model, which was in line with our interpretation in that disease duration of male patients was almost twice the duration of female patients. Meanwhile, no significant association between disease duration and network properties was observed in the subnetwork 2 although the decreased level of connectivity strength was suggested to be associated with the duration of illness in the connections between hub regions [117]. In our results, the level of network segregation was negatively associated with disease duration if the Bonferroni correction was not used. However, there was a lack of literature on the network segregation within the connections between hubs to the best of our knowledge. A negative relationship between age and global efficiency in the subnetwork 2 was reasonable because the integration in hub regions decreases linearly with age [137]. The PANSS score was not significantly associated with the network properties in our study, which might suggest that the disruption of network was rather trait-dependent than state-dependent.

There are some limitations to our study that should be taken into consideration. First, mean FA

in the AMC dataset was significantly higher than in the UCLA dataset after the diffusion MRI harmonization. This was probably because most healthy subjects in the AMC dataset (20 out of 23) were included as a training set whereas 20 healthy subjects from the UCLA dataset were sampled in a random manner. Plus, the multi-site diffusion MRI harmonization required the neuroimaging data to be very well matched for not only age and sex but also socio-economic status and intelligence level, which were not available from the open public databases. Nonetheless, we could minimize the difference of mean FA of the AMC data after the harmonization procedure, thus processing the data more suitable for further analysis. Second, the network properties were adjusted for age, sex, and group in the regression models. Other clinical factors such as intellectual performance [138, 139] or antipsychotics use [140] could affect the measurements, however, such information could not be fully obtained from the database. Third, the goodness-of-fit statistics was lower in the linear mixed-effect model of the robustness simulation of the subnetwork 2. As only 12 nodes were included in the subnetwork 2, a caution should be taken when interpreting the changes of the network measures during the simulation. Fourth, the number of patients with known clinical information was small, thus limiting the generalizability of the clinical correlation analysis. Lastly, we divided the whole structural network into two separate subnetworks experimentally. However, the number of clusters should be better determined when it is calculated optimally [141]. Future studies should consider the optimal number of clusters when investigating subnetworks. Moreover, other clinical features such as fMRI, EEG, other clinical symptom scales, genetic information, or neuroimaging of unaffected relatives could be included in the network examination.

Nevertheless, the strength of our study is that we included a large sample of 189 patients with schizophrenia and 213 healthy controls. Before the network analysis, we performed the quality

control of structural MRIs and integrated DWIs obtained from four different sites through the harmonization procedure. Moreover, we examined the network properties in two distinct subnetworks, which was suggested to be a more appropriate method in terms of small-world property of human brain and the difference of centrality measure observed in schizophrenia. In addition, we simulated the robustness of each subnetwork and investigated the association between the network properties and clinical characteristics to elaborate the structural dysconnectivity in schizophrenia.

5. CONCLUSION

In summary, the structural network of schizophrenia can be divided into two subnetworks based on nodal betweenness centrality. The central subnetwork was less integrated and segregated whereas the non-central subnetwork was more segregated, stronger, and vulnerable to targeted damages. The disrupted connectivity in the non-central subnetwork was significantly associated with disease duration. We conclude that the integration, segregation, and robustness of structural network in schizophrenia are differently manifested between central and non-central subnetworks.

Acknowledgments

The public neuroimaging data used in this study were obtained from the Neuromorphometry by Computer Algorithm Chicago dataset (funded by NIMH grant R01MH056584), the Center for Biomedical Research Excellence (NIH COBRE grant 1P20RR021938), and the Consortium for Neuropsychiatric Phenomics (NIH Roadmap for Medical Research grants UL1-DE019580, RL1MH083268, RL1MH083269, RL1DA024853, RL1MH083270, RL1LM009833, PL1MH083271, and PL1NS062410). Our work was funded by the National Research Foundation of Korea grant (NRF-2012R1A1A1006514, and NRF-2017R1D1A1B03032707).

REFERENCES

1. American Psychiatric Association. (2013). Diagnostic and statistical manual of mental disorders (5th ed.). Arlington, VA.
2. Wernicke C. (1906). Grundriss der Psychiatrie in klinischen Vorlesungen. Liepzig: Georg Thieme.
3. Bleuler E. (1950). Dementia praecox or the group of schizophrenias. International Universities Press.
4. McGuire P, Frith C. Disordered functional connectivity in schizophrenia1. Psychol Med. 1996;26(4):663-7.
5. Lawrie SM, Buechel C, Whalley HC, Frith CD, Friston KJ, Johnstone EC. Reduced frontotemporal functional connectivity in schizophrenia associated with auditory hallucinations. Biol Psychiatry. 2002;51(12):1008-11.
6. Friston K, Liddle P, Frith C, Hirsch S, Frackowiak R. The left medial temporal region and schizophrenia: a PET study. Brain. 1992;115(2):367-82.
7. Breakspear M, Terry JR, Friston KJ, Harris AW, Williams LM, Brown K, et al. A disturbance of nonlinear interdependence in scalp EEG of subjects with first episode schizophrenia. Neuroimage. 2003;20(1):466-78.
8. Friston KJ, Frith CD. Schizophrenia: a disconnection syndrome? Clin Neurosci. 1995;3(2):89-97.
9. Friston KJ. The disconnection hypothesis. Schizophr Res. 1998;30(2):115-25.
10. Lynall ME, Bassett DS, Kerwin R, McKenna PJ, Kitzbichler M, Muller U, et al. Functional connectivity and brain networks in schizophrenia. J Neurosci. 2010;30(28):9477-87.
11. Öngür D, Lundy M, Greenhouse I, Shinn AK, Menon V, Cohen BM, et al. Default mode network abnormalities in bipolar disorder and schizophrenia. Psychiatry Res. Neuroimaging. 2010;183(1):59-68.
12. Camchong J, MacDonald Ⅲ AW, Bell C, Mueller BA, Lim KO. Altered functional and anatomical connectivity in schizophrenia. Schizophr Bull. 2011;37(3):640-50.
13. Oh JS, Kubicki M, Rosenberger G, Bouix S, Levitt JJ, McCarley RW, et al. Thalamo-frontal white matter alterations in chronic schizophrenia: A quantitative diffusion tractography study. Hum Brain Mapp. 2009;30(11):3812-25.
14. Kubicki M, Styner M, Bouix S, Gerig G, Markant D, Smith K, et al. Reduced interhemispheric connectivity in schizophrenia-tractography based segmentation of the corpus callosum. Schizophr Res. 2008;106(2-3):125-31.
15. Phillips OR, Nuechterlein KH, Clark KA, Hamilton LS, Asarnow RF, Hageman NS, et al. Fiber tractography reveals disruption of temporal lobe white matter tracts in schizophrenia. Schizophr Res. 2009;107(1):30-8.

16. Rotarska-Jagiela A, Schönmeyer R, Oertel V, Haenschel C, Vogeley K, Linden DE. The corpus callosum in schizophrenia-volume and connectivity changes affect specific regions. Neuroimage. 2008;39(4):1522-32.
17. Shim G, Oh JS, Jung WH, Jang JH, Choi C-H, Kim E, et al. Altered resting-state connectivity in subjects at ultra-high risk for psychosis: an fMRI study. Behav Brain Funct. 2010;6(1):1-11.
18. Karlsgodt KH, Niendam TA, Bearden CE, Cannon TD. White matter integrity and prediction of social and role functioning in subjects at ultra-high risk for psychosis. Biol Psychiatry. 2009;66(6):562-9.
19. Zhou Y, Liang M, Jiang T, Tian L, Liu Y, Liu Z, et al. Functional dysconnectivity of the dorsolateral prefrontal cortex in first-episode schizophrenia using resting-state fMRI. Neurosci Lett. 2007;417(3):297-302.
20. Luck D, Buchy L, Czechowska Y, Bodnar M, Pike GB, Campbell JS, et al. Fronto-temporal disconnectivity and clinical short-term outcome in first episode psychosis: a DTI-tractography study. J Psychiatr Res. 2011;45(3):369-77.
21. Huisman TAGM. Diffusion-weighted and diffusion tensor imaging of the brain, made easy. Cancer Imaging. 2010;10(1A):S163-S71.
22. Basser PJ, Pierpaoli C. Microstructural and physiological features of tissues elucidated by quantitative-diffusion-tensor MRI. J Magn Reson B. 1996;111(3):209-19.
23. Basser PJ, Pajevic S, Pierpaoli C, Duda J, Aldroubi A. In vivo fiber tractography using DT-MRI data. Magn Reson Med. 2000;44(4):625-32.
24. Beaulieu C, Allen PS. Determinants of anisotropic water diffusion in nerves. Magn Reson Med. 1994;31(4):394-400.
25. Joo SW, Kim H, Jo YT, Ahn S, Choi YJ, Park S, et al. White matter impairments in patients with schizophrenia: A multisite diffusion MRI study. Prog Neuropsychopharmacol Biol Psychiatry. 2021;111:110381.
26. Joo SW, Kim H, Jo YT, Yoon W, Kim Y, Lee J. Shared and distinct white matter abnormalities in schizophrenia and bipolar disorder. Prog Neuropsychopharmacol Biol Psychiatry. 2021;108:110175.
27. Jo YT, Lee J, Joo SW, Kim H, Shon SH, Yoon W, et al. Additive Burden of Abnormal Diffusivity in the Brain with Schizophrenia: A Diffusion Tensor Imaging Study with Public Neuroimaging Data. Psychiat Invest. 2020;17(4):341-49.
28. Kim H, Shon SH, Joo SW, Yoon W, Lee JH, Hur JW, et al. Gray Matter Microstructural Abnormalities and Working Memory Deficits in Individuals with Schizophrenia. Psychiatry Investig. 2019;16(3):234-43.
29. Joo SW, Yoon W, Shon SH, Kim H, Cha S, Park KJ, et al. Altered white matter connectivity in patients with schizophrenia: An investigation using public neuroimaging data from SchizConnect. Plos One. 2018;13(10).
30. Shon SH, Yoon W, Kim H, Joo SW, Kim Y, Lee J. Deterioration in Global Organization of

Structural Brain Networks in Schizophrenia: A Diffusion MRI Tractography Study. Front Psychiatry. 2018;9:272.
31. Lee J, Chon MW, Kim H, Rathi Y, Bouix S, Shenton ME, et al. Diagnostic value of structural and diffusion imaging measures in schizophrenia. Neuroimage Clin. 2018;18:467-74.
32. Joo SW, Chon MW, Rathi Y, Shenton ME, Kubicki M, Lee J. Abnormal asymmetry of white matter tracts between ventral posterior cingulate cortex and middle temporal gyrus in recent-onset schizophrenia. Schizophr Res. 2018;192:159-66.
33. Lee JS, Kim CY, Joo YH, Newell D, Bouix S, Shenton ME, et al. Increased diffusivity in gray matter in recent onset schizophrenia is associated with clinical symptoms and social cognition. Schizophr Res. 2016;176(2-3):144-150.
34. Behrens TE, Woolrich MW, Jenkinson M, Johansen-Berg H, Nunes RG, Clare S, et al. Characterization and propagation of uncertainty in diffusion-weighted MR imaging. Magn Reson Med. 2003;50(5):1077-88.
35. Johnsonbaugh R. (2018). Discrete mathematics (8th ed.). Pearson Education, Inc..
36. Sylvester JJ. Chemistry and Algebra. Nature. 1878;17(432):284.
37. König D. (1990). Theory of finite and infinite graphs. Springer.
38. Stuart JM, Segal E, Koller D, Kim SK. A gene-coexpression network for global discovery of conserved genetic modules. Science. 2003;302(5643):249-55.
39. Shenton ME, Dickey CC, Frumin M, McCarley RW. A review of MRI findings in schizophrenia. Schizophr Res. 2001;49(1-2):1-52.
40. van den Heuvel MP, Fornito A. Brain networks in schizophrenia. Neuropsychol Rev. 2014;24(1):32-48.
41. Hilgetag CC, Burns GA, O'Neill MA, Scannell JW, Young MP. Anatomical connectivity defines the organization of clusters of cortical areas in the macaque monkey and the cat. Philos Trans R Soc Lond B Biol Sci. 2000;355(1393):91-110.
42. Zalesky A, Fornito A, Seal ML, Cocchi L, Westin CF, Bullmore ET, et al. Disrupted axonal fiber connectivity in schizophrenia. Biol Psychiatry. 2011;69(1):80-9.
43. van den Heuvel MP, Sporns O, Collin G, Scheewe T, Mandl RCW, Cahn W, et al. Abnormal Rich Club Organization and Functional Brain Dynamics in Schizophrenia. JAMA Psychiatry. 2013;70(8):783-92.
44. van den Heuvel MP, Mandl RC, Stam CJ, Kahn RS, Hulshoff Pol HE. Aberrant frontal and temporal complex network structure in schizophrenia: a graph theoretical analysis. J Neurosci. 2010;30(47):15915-26.
45. Zhang Y, Lin L, Lin CP, Zhou Y, Chou KH, Lo CY, et al. Abnormal topological organization of structural brain networks in schizophrenia. Schizophr Res. 2012;141(2-3):109-18.
46. Wang QF, Su TP, Zhou Y, Chou KH, Chen IY, Jiang TZ, et al. Anatomical insights into disrupted small-world networks in schizophrenia. Neuroimage. 2012;59(2):1085-93.

47. Griffa A, Baumann PS, Thiran JP, Hagmann P. Structural connectomics in brain diseases. Neuroimage. 2013;80:515-26.
48. Bassett DS, Bullmore E, Verchinski BA, Mattay VS, Weinberger DR, Meyer-Lindenberg A. Hierarchical organization of human cortical networks in health and schizophrenia. J Neurosci. 2008;28(37):9239-48.
49. Rubinov M, Bullmore E. Schizophrenia and abnormal brain network hubs. Dialogues Clin Neurosci. 2013;15(3):339-49.
50. G Jeong JK. A Review of Structural Brain Networks Study: Schizophrenia. Journal of the Korean Society of Imaging Informatics in Medicine. 2017;23:21-7.
51. Crossley NA, Mechelli A, Scott J, Carletti F, Fox PT, McGuire P, et al. The hubs of the human connectome are generally implicated in the anatomy of brain disorders. Brain. 2014;137(Pt 8):2382-95.
52. Kambeitz J, Kambeitz-Ilankovic L, Cabral C, Dwyer DB, Calhoun VD, van den Heuvel MP, et al. Aberrant Functional Whole-Brain Network Architecture in Patients With Schizophrenia: A Meta-analysis. Schizophr Bull. 2016;42 Suppl 1:S13-21.
53. Micheloyannis S, Pachou E, Stam CJ, Breakspear M, Bitsios P, Vourkas M, et al. Small-world networks and disturbed functional connectivity in schizophrenia. Schizophr Res. 2006;87(1-3):60-6.
54. Rubinov M, Knock SA, Stam CJ, Micheloyannis S, Harris AW, Williams LM, et al. Small-world properties of nonlinear brain activity in schizophrenia. Hum Brain Mapp. 2009;30(2):403-16.
55. Liu Y, Liang M, Zhou Y, He Y, Hao Y, Song M, et al. Disrupted small-world networks in schizophrenia. Brain. 2008;131(Pt 4):945-61.
56. Meskaldji DE, Ottet MC, Cammoun L, Hagmann P, Meuli R, Eliez S, et al. Adaptive strategy for the statistical analysis of connectomes. PLoS One. 2011;6(8):e23009.
57. Sporns O, Honey CJ. Small worlds inside big brains. Proc Natl Acad Sci U S A. 2006;103(51):19219-20.
58. Zhao X, Tian L, Yan J, Yue WH, Yan H, Zhang D. Abnormal Rich-Club Organization Associated with Compromised Cognitive Function in Patients with Schizophrenia and Their Unaffected Parents. Neurosci Bull. 2017;33(4):445-54.
59. Newman ME. Spectral methods for community detection and graph partitioning. Phys Rev E Stat Nonlin Soft Matter Phys. 2013;88(4):042822.
60. Karrer B, Newman ME. Stochastic blockmodels and community structure in networks. Phys Rev E Stat Nonlin Soft Matter Phys. 2011;83(1 Pt 2):016107.
61. Lu X, Szymanski BK. A Regularized Stochastic Block Model for the robust community detection in complex networks. Sci Rep. 2019;9(1):13247.
62. Atluri G, Steinbach M, Lim KO, Kumar V, MacDonald A, 3rd. Connectivity cluster analysis for discovering discriminative subnetworks in schizophrenia. Hum Brain Mapp. 2015;36(2):756-67.
63. Wang H, Zeng LL, Chen Y, Yin H, Tan Q, Hu D. Evidence of a dissociation pattern in default

mode subnetwork functional connectivity in schizophrenia. Sci Rep. 2015;5:14655.
64. Baker JT, Dillon DG, Patrick LM, Roffman JL, Brady RO, Jr., Pizzagalli DA, et al. Functional connectomics of affective and psychotic pathology. Proc Natl Acad Sci U S A. 2019;116(18):9050-9.
65. Xiang B, Wang Q, Lei W, Li M, Li Y, Zhao L, et al. Genes in immune pathways associated with abnormal white matter integrity in first-episode and treatment-naive patients with schizophrenia. Br J Psychiatry. 2019;214(5):281-7.
66. Bartlett TE, Muller S, Diaz A. Single-cell Co-expression Subnetwork Analysis. Sci Rep. 2017;7(1):15066.
67. Drakesmith M, Caeyenberghs K, Dutt A, Zammit S, Evans CJ, Reichenberg A, et al. Schizophrenia-like topological changes in the structural connectome of individuals with subclinical psychotic experiences. Hum Brain Mapp. 2015;36(7):2629-43.
68. Schirmer MD, Chung AW, Grant PE, Rost NS. Network structural dependency in the human connectome across the life-span. Netw Neurosci. 2019;3(3):792-806.
69. Alloza C, Bastin ME, Cox SR, Gibson J, Duff B, Semple SI, et al. Central and non-central networks, cognition, clinical symptoms, and polygenic risk scores in schizophrenia. Hum Brain Mapp. 2017;38(12):5919-30.
70. Cheng H, Newman S, Goni J, Kent JS, Howell J, Bolbecker A, et al. Nodal centrality of functional network in the differentiation of schizophrenia. Schizophr Res. 2015;168(1-2):345-52.
71. Singh M, Science GBCfS, Jodhpur IIoT, India, Information DAIo, Technology C, et al. Network biomarkers of schizophrenia by graph theoretical investigations of Brain Functional Networks. arXiv: Quantitative Methods. 2016.
72. Gorgolewski KJ, Durnez J, Poldrack RA. Preprocessed Consortium for Neuropsychiatric Phenomics dataset. F1000Res. 2017;6:1262.
73. Wang L, Alpert KI, Calhoun VD, Cobia DJ, Keator DB, King MD, et al. SchizConnect: Mediating neuroimaging databases on schizophrenia and related disorders for large-scale integration. Neuroimage. 2016;124(Pt B):1155-67.
74. Billah TN, Isaiah; Rathi, Yogesh; Bouix, Sylvain, Come, Carquex. Slicer Diffusion QC Tool 2018. [cited 2021 11 Aug]. Available from: https://github.com/pnlbwh/SlicerDiffusionQC.
75. Jenkinson M, Bannister P, Brady M, Smith S. Improved optimization for the robust and accurate linear registration and motion correction of brain images. Neuroimage. 2002;17(2):825-41.
76. Jenkinson M, Smith S. A global optimisation method for robust affine registration of brain images. Med Image Anal. 2001;5(2):143-56.
77. Desikan RS, Segonne F, Fischl B, Quinn BT, Dickerson BC, Blacker D, et al. An automated labeling system for subdividing the human cerebral cortex on MRI scans into gyral based regions of interest. Neuroimage. 2006;31(3):968-80.
78. Fischl B, van der Kouwe A, Destrieux C, Halgren E, Segonne F, Salat DH, et al. Automatically parcellating the human cerebral cortex. Cereb Cortex. 2004;14(1):11-22.

79. Fischer B, Modersitzki J, editors. (2003). FLIRT: A Flexible Image Registration Toolbox. Berlin, Heidelberg: Springer Berlin Heidelberg.
80. Billah T, Cetin Karayumak S, Bouix S, Rathi Y. Multi-site Diffusion MRI Harmonization. 2019 [cited 2021 12 Aug]. Available from: https://github.com/pnlbwh/dMRIharmoniziation.
81. Cetin Karayumak S, Bouix S, Ning L, James A, Crow T, Shenton M, et al. Retrospective harmonization of multi-site diffusion MRI data acquired with different acquisition parameters. Neuroimage. 2019;184:180-200.
82. Mirzaalian H, Ning L, Savadjiev P, Pasternak O, Bouix S, Michailovich O, et al. Multi-site harmonization of diffusion MRI data in a registration framework. Brain Imaging Behav. 2018;12(1):284-95.
83. Kellner E, Dhital B, Kiselev VG, Reisert M. Gibbs-ringing artifact removal based on local subvoxel-shifts. Magn Reson Med. 2016;76(5):1574-81.
84. Zhang S, Arfanakis K. Evaluation of standardized and study-specific diffusion tensor imaging templates of the adult human brain: Template characteristics, spatial normalization accuracy, and detection of small inter-group FA differences. Neuroimage. 2018;172:40-50.
85. Jenkinson M, Beckmann CF, Behrens TE, Woolrich MW, Smith SM. FSL. Neuroimage. 2012;62(2):782-90.
86. Jbabdi S, Johansen-Berg H. Tractography: where do we go from here? Brain Connect. 2011;1(3):169-83.
87. Descoteaux M, Deriche R, Knosche TR, Anwander A. Deterministic and probabilistic tractography based on complex fibre orientation distributions. IEEE Trans Med Imaging. 2009;28(2):269-86.
88. Behrens TEJ, Berg HJ, Jbabdi S, Rushworth MFS, Woolrich MW. Probabilistic diffusion tractography with multiple fibre orientations: What can we gain? Neuroimage. 2007;34(1):144-55.
89. Rubinov M, Sporns O. Complex network measures of brain connectivity: uses and interpretations. Neuroimage. 2010;52(3):1059-69.
90. van den Heuvel MP, Stam CJ, Boersma M, Hulshoff Pol HE. Small-world and scale-free organization of voxel-based resting-state functional connectivity in the human brain. Neuroimage. 2008;43(3):528-39.
91. Achard S, Bullmore E. Efficiency and cost of economical brain functional networks. PLoS Comput Biol. 2007;3(2):e17.
92. Hagmann P, Kurant M, Gigandet X, Thiran P, Wedeen VJ, Meuli R, et al. Mapping Human Whole-Brain Structural Networks with Diffusion MRI. PLoS One. 2007;2(7):e597.
93. Haak KV, Beckmann CF. Objective analysis of the topological organization of the human cortical visual connectome suggests three visual pathways. Cortex. 2018;98:73-83.
94. Latora V, Marchiori M. Efficient behavior of small-world networks. Phys Rev Lett. 2001;87(19):198701.

95. Freeman LC. A set of measures of centrality based on betweenness. Sociometry. 1977:35-41.
96. Watts DJ, Strogatz SH. Collective dynamics of 'small-world' networks. Nature. 1998;393(6684):440-2.
97. Cao Q, Shu N, An L, Wang P, Sun L, Xia MR, et al. Probabilistic diffusion tractography and graph theory analysis reveal abnormal white matter structural connectivity networks in drug-naive boys with attention deficit/hyperactivity disorder. J Neurosci. 2013;33(26):10676-87.
98. Jain M, Verma C. Adapting k-means for Clustering in Big Data. Int J Comput Appl. 2014;101(1):19-24.
99. Skudlarski P, Jagannathan K, Anderson K, Stevens MC, Calhoun VD, Skudlarska BA, et al. Brain Connectivity Is Not Only Lower but Different in Schizophrenia: A Combined Anatomical and Functional Approach. Biol Psychiatry. 2010;68(1):61-9.
100. Kaiser M, Martin R, Andras P, Young MP. Simulation of robustness against lesions of cortical networks. Eur J Neurosci. 2007;25(10):3185-92.
101. Kay SR, Fiszbein A, Opler LA. The positive and negative syndrome scale (PANSS) for schizophrenia. Schizophr Bull. 1987;13(2):261-76.
102. Leucht S, Samara M, Heres S, Patel MX, Furukawa T, Cipriani A, et al. Dose Equivalents for Second-Generation Antipsychotic Drugs: The Classical Mean Dose Method. Schizophr Bull. 2015;41(6):1397-402.
103. R Core Team (2018): A language and environment for statistical computing. R Foundation for Statistical Computing, Vienna. Available from: https://www.R-project.org.
104. Dimulescu C, Gareayaghi S, Kamp F, Fromm S, Obermayer K, Metzner C. Structural Differences Between Healthy Subjects and Patients With Schizophrenia or Schizoaffective Disorder: A Graph and Control Theoretical Perspective. Front Psychiatry. 2021;12:669783.
105. van Dellen E, Bohlken MM, Draaisma L, Tewarie PK, van Lutterveld R, Mandl R, et al. Structural Brain Network Disturbances in the Psychosis Spectrum. Schizophr Bull. 2016;42(3):782-9.
106. Krukow P, Jonak K, Karpinski R, Karakula-Juchnowicz H. Abnormalities in hubs location and nodes centrality predict cognitive slowing and increased performance variability in first-episode schizophrenia patients. Sci Rep. 2019;9(1):9594.
107. Gong GL, He Y, Concha L, Lebel C, Gross DW, Evans AC, et al. Mapping Anatomical Connectivity Patterns of Human Cerebral Cortex Using In Vivo Diffusion Tensor Imaging Tractography. Cereb Cortex. 2009;19(3):524-36.
108. Sporns O, Honey CJ, Kotter R. Identification and classification of hubs in brain networks. PLoS One. 2007;2(10):e1049.
109. Hagmann P, Cammoun L, Gigandet X, Meuli R, Honey CJ, Wedeen VJ, et al. Mapping the structural core of human cerebral cortex. PLoS Biol. 2008;6(7):e159.

110. van den Heuvel MP, Sporns O. Network hubs in the human brain. Trends Cogn Sci. 2013;17(12):683-96.
111. Xia MR, Lin QX, Bi YC, He Y. Connectomic Insights into Topologically Centralized Network Edges and Relevant Motifs in the Human Brain. Front Hum Neurosci. 2016;10:158.
112. Oldham S, Fornito A. The development of brain network hubs. Dev Cogn Neurosci. 2019;36:100607.
113. Colizza V, Flammini A, Serrano MA, Vespignani A. Detecting rich-club ordering in complex networks. Nature Physics. 2006;2(2):110-5.
114. Ottet MC, Schaer M, Debbane M, Cammoun L, Thiran JP, Eliez S. Graph theory reveals dysconnected hubs in 22q11DS and altered nodal efficiency in patients with hallucinations. Front Hum Neurosci. 2013;7:402.
115. van den Heuvel MP, Kahn RS, Goni J, Sporns O. High-cost, high-capacity backbone for global brain communication. Proc Natl Acad Sci U S A. 2012;109(28):11372-7.
116. Shi F, Yap P-T, Gao W, Lin W, Gilmore JH, Shen D. Altered structural connectivity in neonates at genetic risk for schizophrenia: a combined study using morphological and white matter networks. NeuroImage. 2012;62(3):1622-33.
117. Collin G, Kahn RS, de Reus MA, Cahn W, van den Heuvel MP. Impaired rich club connectivity in unaffected siblings of schizophrenia patients. Schizophr Bull. 2014;40(2):438-48.
118. Colombo C, Bonfanti A, Scarone S. Anatomical Characteristics of the Corpus Callosum and Clinical Correlates in Schizophrenia. Eur Arch Psy Clin N. 1994;243(5):244-8.
119. Innocenti GM, Ansermet F, Parnas J. Schizophrenia, neurodevelopment and corpus callosum. Mol Psychiatry. 2003;8(3):261-74.
120. Foong J, Maier M, Clark CA, Barker GJ, Miller DH, Ron MA. Neuropathological abnormalities of the corpus callosum in schizophrenia: a diffusion tensor imaging study. J Neurol Neurosurg Psychiatry. 2000;68(2):242-4.
121. Agartz I, Andersson JL, Skare S. Abnormal brain white matter in schizophrenia: a diffusion tensor imaging study. Neuroreport. 2001;12(10):2251-4.
122. Leow A, Ajilore O, Zhan L, Arienzo D, GadElkarim J, Zhang A, et al. Impaired inter-hemispheric integration in bipolar disorder revealed with brain network analyses. Biol Psychiatry. 2013;73(2):183-93.
123. Griffa A, Baumann PS, Ferrari C, Do KQ, Conus P, Thiran JP, et al. Characterizing the connectome in schizophrenia with diffusion spectrum imaging. Hum Brain Mapp. 2015;36(1):354-66.
124. Griffa A, Baumann PS, Klauser P, Mullier E, Cleusix M, Jenni R, et al. Brain connectivity alterations in early psychosis: from clinical to neuroimaging staging. Transl Psychiatry. 2019;9(1):62.
125. Bernard JA, Russell CE, Newberry RE, Goen JRM, Mittal VA. Patients with schizophrenia show aberrant patterns of basal ganglia activation: Evidence from ALE meta-analysis. Neuroimage Clin. 2017;14:450-63.

126. Zhang H, Wei X, Tao H, Mwansisya TE, Pu W, He Z, et al. Opposite effective connectivity in the posterior cingulate and medial prefrontal cortex between first-episode schizophrenic patients with suicide risk and healthy controls. PLoS One. 2013;8(5):e63477.
127. Rubinov M, Sporns O, van Leeuwen C, Breakspear M. Symbiotic relationship between brain structure and dynamics. Bmc Neurosci. 2009;10:55.
128. Fornito A, Bullmore ET. Reconciling abnormalities of brain network structure and function in schizophrenia. Curr Opin Neurobiol. 2015;30:44-50.
129. Wylie KP, Tregellas JR. The role of the insula in schizophrenia. Schizophr Res. 2010;123(2-3):93-104.
130. Lindner C, Dannlowski U, Walhofer K, Rodiger M, Maisch B, Bauer J, et al. Social alienation in schizophrenia patients: association with insula responsiveness to facial expressions of disgust. PLoS One. 2014;9(1):e85014.
131. Zhang R, Wei Q, Kang Z, Zalesky A, Li M, Xu Y, et al. Disrupted brain anatomical connectivity in medication-naive patients with first-episode schizophrenia. Brain Struct Funct. 2015;220(2):1145-59.
132. Lo CYZ, Su TW, Huang CC, Hung CC, Chen WL, Lan TH, et al. Randomization and resilience of brain functional networks as systems-level endophenotypes of schizophrenia. P Natl Acad Sci USA. 2015;112(29):9123-8.
133. Alexander-Bloch AF, Gogtay N, Meunier D, Birn R, Clasen L, Lalonde F, et al. Disrupted modularity and local connectivity of brain functional networks in childhood-onset schizophrenia. Front Syst Neurosci. 2010;4:147.
134. Palaniyappan L. Progressive cortical reorganisation: A framework for investigating structural changes in schizophrenia. Neurosci Biobehav Rev. 2017;79:1-13.
135. Vita A, De Peri L, Deste G, Sacchetti E. Progressive loss of cortical gray matter in schizophrenia: a meta-analysis and meta-regression of longitudinal MRI studies. Transl Psychiatry. 2012;2:e190.
136. Andreasen NC, Nopoulos P, Magnotta V, Pierson R, Ziebell S, Ho BC. Progressive brain change in schizophrenia: a prospective longitudinal study of first-episode schizophrenia. Biol Psychiatry. 2011;70(7):672-9.
137. Zhao T, Cao M, Niu H, Zuo XN, Evans A, He Y, et al. Age-related changes in the topological organization of the white matter structural connectome across the human lifespan. Hum Brain Mapp. 2015;36(10):3777-92.
138. Li Y, Liu Y, Li J, Qin W, Li K, Yu C, et al. Brain anatomical network and intelligence. PLoS Comput Biol. 2009;5(5):e1000395.
139. van den Heuvel MP, Stam CJ, Kahn RS, Hulshoff Pol HE. Efficiency of functional brain networks and intellectual performance. J Neurosci. 2009;29(23):7619-24.
140. Towlson EK, Vertes PE, Muller-Sedgwick U, Ahnert SE. Brain Networks Reveal the Effects of

Antipsychotic Drugs on Schizophrenia Patients and Controls. Front Psychiatry. 2019;10:611.
141. Tenenbaum JB, de Silva V, Langford JC. A global geometric framework for nonlinear dimensionality reduction. Science. 2000;290(5500):2319-23.

국문요약

배경: 조현병의 연결성 장애는 네트워크 분석을 통해 증명할 수 있다. 뇌가 작은 세상 네트워크의 집합체라는 점과 특정 뇌 구역에 국한된 이상 소견이 조현병의 발생 기전을 설명할 수 없다는 점 때문에 구조연결성은 더 작은 서브네트워크 단위에서 연구되어야 한다.

목표: 조현병의 구조연결성 장애를 두 개의 서브네트워크 단위에서 분석하고자 한다.

방법: 공공 데이터베이스를 이용해 뇌확산 영상으로 구조 네트워크를 구성한다. 노드 단위에서의 매개 중심성을 기준으로 k-means 알고리즘으로 두 개의 서브네트워크를 구성한다. 각 서브네트워크에서 환자군과 대조군의 네트워크 지표를 비교하고 견고성 시뮬레이션과 임상 지표와의 관련성을 분석한다.

결과: 1번 서브네트워크는 75개의 ROI로 구성되고 2번 서브네트워크는 중심성이 높은 12개의 ROI로 구성되었다. 로컬 효율성, 클러스터링 계수, 전반적 연결성은 1번 서브네트워크에서 환자가 더 높았는데 이들 지표와 글로벌 효율성이 2번 서브네트워크에서는 환자가 더 낮았다. 조현병 환자의 1번 서브네트워크가 연속적 데미지에는 더 견고하였고 1번 서브네트워크에서 상승한 3개의 지표는 유병 기간과 음의 상관을 보였다.

결론: 높은 중심성 서브네트워크는 분리와 통합 정도가 낮았으며 낮은 중심성 서브네트워크는 분리와 연결 정도가 높고 데미지에 견고했다. 낮은 중심성 네트워크의 구조연결성 장애는 유병 기간과 연관되어 있다. 따라서, 조현병 환자의 구조 연결성은 높은 중심성과 낮은 중심성 서브네트워크에서 다르게 나타난다.